HERON contains contributions based mainly on research work performed in I.B.B.C. and STEVIN and related to strength of materials and structures and materials science.

Jointly edited by:

STEVIN-LABORATORY
of the Department of
Civil Engineering of the
Delft University of Technology,
Delft, The Netherlands
and
I.B.B.C. INSTITUTE TNO
for Building Materials
and Building Structures,
Rijswijk (ZH), The Netherlands.

Secretary:

G. J. van Alphen
Stevinweg 1
P.O. Box 5048
2600 GA Delft, The Netherlands

HERON vol. 25
1980
no. 2

Contents

COLLAPSE ANALYSIS OF THREE DIMENSIONAL ASSEMBLAGES OF ECCENTRICALLY STIFFENED HOT ROLLED STEEL PLATES AND SHALLOW SHELLS

Dr. R. S. Puthli, C.Eng., M.I.C.E.

Publications in HERON since 1970

COLLAPSE ANALYSIS OF THREE DIMENSIONAL ASSEMBLAGES OF ECCENTRICALLY STIFFENED HOT ROLLED STEEL PLATES AND SHALLOW SHELLS

Synopsis

This paper describes a finite element formulation of the large-deflection, elasto-plastic behaviour of eccentrically stiffened steel plated assemblages in more than one plane. The theory is based on a lagrangian formulation for moderately large deflections, using rectangular plate elements and stiffener line elements that may be given initial deformations and slopes to form shallow shells. Plasticity in the plate is treated using Ilyushin's yield criterion, whereas a simple uniaxial yield criterion is adopted for the stiffeners. Torsional stiffness of the stiffeners is treated in a linear-elastic manner and torsional instability (stiffener tripping) is not considered.

A computer program (CASPA) has been developed for the analysis. Classical, numerical and experimental examples are compared with numerical solutions obtained from computer analyses. The numerical solutions commence with geometric imperfections at zero load, with an incremental approach upto collapse.

Collapse analysis of three dimensional assemblages of eccentrically stiffened hot rolled steel plates and shallow shells

1 Introduction

Theoretical investigations on large deflection, elasto-plastic collapse behaviour of stiffened and unstiffened plates have, in the past, been restricted to individual components with idealised boundary conditions [1-8]. In order to investigate the behaviour of real structures upto collapse, groups of such components require consideration, especially in the highly stressed regions, where interaction between the components is inevitable and likely to be significant. Some work has already been done on plated (unstiffened) assemblages by the author and other investigators [9-14].

The present formulation is capable of analysing the behaviour of stiffened plate assemblages in steel structures using hot rolled steel plates and sections, where non-linear buckling coupled with a linear elastic and perfectly plastic stress strain relationship (no strain hardening) may be encountered. Comparisons with other theoretical and experimental results [1, 4, 12, 15] have shown a correlation that is satisfactory to engineering accuracy. Major areas of application are in offshore structures, bridges and ship construction.

The analysis procedure utilises the well known displacement formulation and provides a highly accurate mathematical model for general application to eccentrically stiffened plate assemblages, orientated in more than one plane.

The plates and stiffeners are capable of membrane and flexural action. The structure is modelled using rectangular elements for the plate and line elements for the stiffeners. Both element types may be eccentric to the line of action of the forces (or datum line).

Bilinear shape functions are used for the in-plane displacement field, while the restricted quartic shape functions which pass the patch test are used for the out-of-plane deflections of the plate element. The stiffener element is represented by a linear shape function for the in-plane displacements and a cubic shape function for the out-of-plane deflections.

Plasticity in the plate is treated using Ilyushin's yield criterion [16], which is a direct function of the six stress resultants.

It is therefore unnecessary to divide the plate into layers, where heavier demands are made on computer time and storage. Ilyushin's yield criterion is approximate for bending dominant cases because it does not account for "intermediate" plasticity between first fibre yield and full plasticity of the cross-section. However, as mentioned above, the solutions obtained have been acceptable with regard to engineering accuracy. Plasticity in the stiffener is treated by using a simple uniaxial yield criterion where the effect of torsion is ignored, so that the stiffener does not require to be divided into layers. This gives an added saving in computer time and storage. This simplification is obtained by not allowing for elastic unloading of the stiffeners in the plastic stages. The yield crite-

rion for the stiffeners requires modification if the computer program CASPA is to be applied to structures where elastic unloading of the stiffeners will be encountered.

2 Basic assumptions

The approximations are based on the assumptions that

1. The plate element is thin;
2. Plane sections remain plane - Bernoulli-Euler-Kirchoff hypothesis;
3. The transverse normal stress is negligible;
4. A Lagrangian (initial coordinate) system is used. Furthermore, the slopes $\partial w/\partial x$, $\partial w/\partial y$ in the elements should be small ($\ll 1$);
5. The material stress strain relationship is linear elastic and perfectly plastic (no strain hardening).
6. Torsion in the stiffener is treated in a linear-elastic manner.

The first assumption does not permit transverse shear deformation of the plate, which is included only in thick plate theory. The second and third assumptions allow normals to the mid-plane of the plate and stiffener to remain normal to it, with no change in length under deformation. Therefore, all strain components normal to the mid-surface vanish and no shear deformation occurs.

The fourth assumption permits the referencing of all derivatives and calculations to the original undeformed configuration, thereby allowing only moderately large deflections (small slopes). For the fifth assumption, since isotropic material is assumed, only the Young's modulus E, Poisson's ratio v and yield stress σ_0 are required to specify its behaviour. Also, approximate yield criteria based on Von Mises yield criterion are used for the plate and stiffener, as described in 5.1 and 5.2.

The last assumption signifies that in the stiffener element, torsional instability (tripping) is not included and torsional stresses are ignored in the plasticity formulation.

3 Displacement functions

3.1 *Membrane behaviour of the plate element*

The simplest (first order) rectangular element [15, 17] is based on taking the corner nodes (see Fig. 1) and working only with displacements as nodal quantities. The dimensionless local cartesian coordinates (or normalised coordinates, ξ, η) that are used henceforth (with limits of ± 1) are defined as:

$$\begin{aligned} \xi &= (x - x_c)/a, \qquad d\xi = dx/a \\ \eta &= (y - y_c)/b, \qquad d\eta = dy/b \end{aligned} \tag{3.1.1}$$

The area integral is defined as

$$\iint_A g(x,y)\, dA = ab \int_{-1}^{+1} \int_{-1}^{+1} g(\xi,\eta)\, d\xi\, d\eta \tag{3.1.2}$$

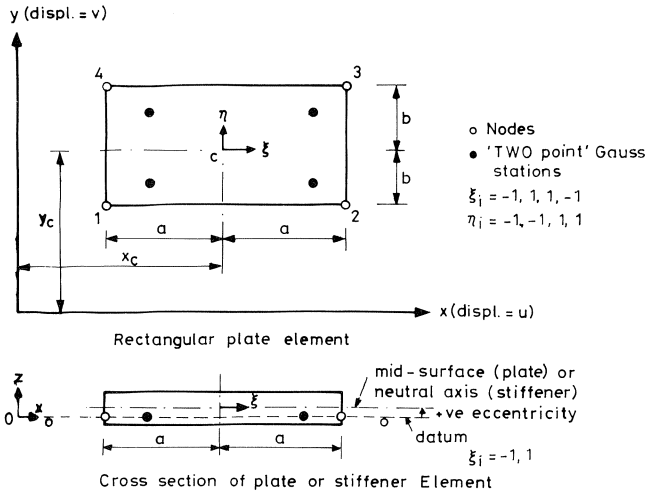

Fig. 1. Element details.

Bilinear in-plane functions for the elements are generated by evaluating

$$\delta(\xi,\eta) = \alpha_1 + \alpha_2\xi + \alpha_3\eta + \alpha_4\xi\eta \tag{3.1.3}$$

at the nodal points and solving for the α. We get

$$\begin{aligned} u(\xi,\eta) &= \{N\}^T\{u\}^e \\ v(\xi,\eta) &= \{N\}^T\{v\}^e \end{aligned} \tag{3.1.4}$$

where $\{u\}^e$, $\{v\}^e$ are the vectors of displacements at the element nodes and

$$N_i = \tfrac{1}{4}(1 + \xi\xi_i)(1 + \eta_i\eta) \tag{3.1.5}$$

where ξ_i, η_i are their respective nodal values for $i = 1,4$ i.e.

$$\begin{aligned} \xi_i &= -1, 1, 1, -1 \\ \eta_i &= -1, -1, 1, 1 \end{aligned}$$

These displacement functions satisfy the compatibility conditions for a general quadrilateral.

3.2 *Membrane behaviour of the stiffener element*

The in-plane displacement function is linear and coincides with that of the plate element along the sides of the plate.

Referring to Fig. 1, and the notations described above,

$$u(\xi) = \{N\}^T\{u\}^e \tag{3.2.1}$$

and

$$N_i = \tfrac{1}{2}(1 + \xi\xi_i) \tag{3.2.2}$$

Where ξ_i is the nodal value for $i = 1,2$ i.e.

$$\xi_i = -1, 1$$

3.3 *Flexural behaviour of the plate element*

The displacement function is the well-known, non-conforming, restricted quartic polynomial for a quadrilateral, chosen by Zienkiewicz and Cheung [18]. The displacement function in normalised coordinates is given by

$$w = \alpha_1 + \alpha_2\xi + \alpha_3\eta + \alpha_4\xi^2 + \alpha_5\xi\eta + \alpha_6\eta^2 + \alpha_7\xi^3 + \alpha_8\xi^2\eta + \alpha_9\xi\eta^2 + \alpha_{10}\eta^3 + \alpha_{11}\xi^3\eta + \alpha_{12}\xi\eta^3 \tag{3.3.1}$$

where α_1 to α_{12} are arbitrary coefficients.

The relationships between the normalised and cartesian coordinates are given in 3.1. Evaluating the expression 3.3.1 at the nodal points and solving for α gives the shape functions derived by Melosh [19].

$$\text{i.e.} \qquad w(\xi,\eta) = \{N\}^T \begin{Bmatrix} w \\ \theta_x \\ \theta_y \end{Bmatrix}^e \tag{3.3.2}$$

where w = lateral plate displacement,

$$\theta_x = -\frac{\partial w}{\partial y},\ \theta_y = \frac{\partial w}{\partial x}$$

(for sign convention and element orientation, refer to Fig. 2 and 3) and the shape function for any node i (with coordinates at the centroid) is

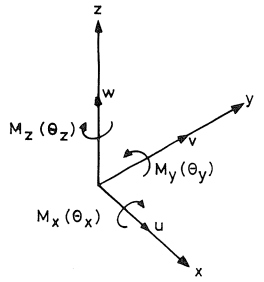

Fig. 2. Sign convention for displacements and external forces in local and global coordinates (directions shown are positive).

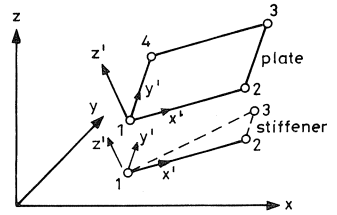

Fig. 3. Orientation of the local element coordinates with respect to the global coordinates.

$$\{N_i\} = \tfrac{1}{8} \begin{Bmatrix} (1+\xi_i\xi)(1+\eta_i\eta)(2+\xi_i\xi+\eta_i\eta-\xi^2-\eta^2) \\ -b\eta_i(1+\xi_i\xi)(1+\eta_i\eta)(\eta^2-1) \\ a\xi_i(1+\xi_i\xi)(1+\eta_i\eta)(\xi^2-1) \end{Bmatrix} \tag{3.3.3}$$

ξ_i and η_i are defined in 3.1.

3.4 *Flexural behaviour of the stiffener element*

In the plate element, at ξ = constant and η = constant, displacement "w" varies as a cubic. The element interfaces where stiffeners may be provided consist of such lines. Therefore, a one dimensional version of the shape function for the plate is used here for compatibility.

$$w(\xi) = \{N\}^T \begin{Bmatrix} w \\ \theta_y \end{Bmatrix}^e \tag{3.4.1}$$

where notations and sign conventions are as for the plate element. The shape function for any node "i" is:

$$\{N_i\} = \tfrac{1}{4} \begin{Bmatrix} 2+3\xi\xi_i-\xi_i\xi^3 \\ a(\xi^2-1)(\xi+\xi_i) \end{Bmatrix} \tag{3.4.2}$$

4 Strain Matrices

Differentiation of the chosen shape functions (derived from the displacement functions) leads to the strain matrices, namely $[H]$ and $[HS]$ (the in-plane strain matrices), $[F]$ and $[FS]$ (the bending curvature matrices), and $[G]$ and $[GS]$ (the slope matrices) which are due to large deflection effects such as $\frac{1}{2}(\partial w/\partial x)^2$, etc. These are the strain-nodal displacement relationships, and are derived for the rectangular and line elements. All the following strain matrices are with reference to the plate and stiffener neutral axis and not the datum. All stresses and strains, modular and stiffness matrices will, however, refer to the datum (see Fig. 1).

4.1 *Strain matrix (in-plane) of the plate element*

Differentiation of equation 3.1.4 leads to:

$$\begin{Bmatrix} \varepsilon_x \\ \varepsilon_y \\ \varepsilon_{xy} \end{Bmatrix} = \begin{Bmatrix} \partial u/\partial x \\ \partial v/\partial y \\ \dfrac{\partial u}{\partial y} + \dfrac{\partial v}{\partial x} \end{Bmatrix} = [H] \begin{Bmatrix} u \\ v \end{Bmatrix}^e \tag{4.1.1}$$

where $[H]$ is the strain matrix. This has, however, been modified so that the shear stress is constant over the element and equal to its centroidal value [20]. This modification is

necessary because otherwise the element becomes too stiff in shear. Also the convergence in the analysis of in plane bending problems is poor. The modified strain matrix is given by

$$[H]=\begin{bmatrix} 1/a\{\frac{1}{4}\xi_i(1+\eta_i\eta)\}^T & 0 \\ 0 & 1/b\{\frac{1}{4}\eta_i(1+\xi_i\xi)\}^T \\ 1/b\{\frac{1}{4}\eta_i\}^T & 1/a\{\frac{1}{4}\xi_i\}^T \end{bmatrix} \tag{4.1.2}$$

where ξ_i, n_i are their respective nodal values for $i=1,4$ i.e.

$$\xi_i=-1,\ 1,\ 1,\ -1$$
$$n_i=-1,\ -1,\ 1,\ 1$$

4.2 *Strain matrix (in-plane) of the stiffener element*

Differentiation of 3.2.1 leads to

$$\varepsilon_x=\partial u/\partial x=[HS]\{u\}^e \tag{4.2.1}$$

where

$$[HS]=\left[\frac{\xi_i}{2a}\right]$$

4.3 *Curvature matrix of the plate element*

Double differentiation of the restricted cubic shape function 3.3.2 gives curvatures χ_x and χ_y that vary linearly with x and y. However, the twisting curvature variation is quadratic, and inconsistent with the lower order (four point Gauss) numerical integration adopted for the stiffness matrix. The curvature term can be reduced simply by under integrating the twisting strain energy with the desired two by two Gaussian integration scheme, instead of the three by three scheme strictly required. However, Crisfield [21] has modified the curvature matrix at source using Reissner's variational principle. The effect is the same as that obtained if the quadratic distribution is replaced by a linear distribution that coincides with the former at four two point Gauss stations. This modification has been used in the present formulation, so that

$$\begin{Bmatrix} \chi_x \\ \chi_y \\ \chi_{xy} \end{Bmatrix}=\begin{Bmatrix} \dfrac{-\partial^2 w}{\partial x^2} \\ \dfrac{-\partial^2 w}{\partial y^2} \\ \dfrac{2\partial^2 w}{\partial x \partial y} \end{Bmatrix}=[F]\begin{Bmatrix} w \\ \theta_x \\ \theta_y \end{Bmatrix} \tag{4.3.1}$$

where

$$\theta_x=-\frac{\partial w}{\partial y},\qquad \theta_y=\frac{\partial w}{\partial x}$$

and

$$[F]=\begin{bmatrix} \left\{\frac{3}{4a^2}\xi_i\xi(1+\eta_i\eta)\right\}^T & 0 & \left\{-\frac{1}{4a}(1+\eta_i\eta)(3\xi+\xi_i)\right\}^T \\ \left\{\frac{3}{4b^2}\eta_i\eta(1+\xi_i\xi)\right\}^T & \left\{\frac{1}{4b}(1+\xi_i\xi)(3\eta+\eta_i)\right\}^T & 0 \\ \left\{\frac{1}{2ab}\xi_i\eta_i\right\}^T & \left\{-\frac{1}{2a}\xi_i\eta_i\eta\right\}^T & \left\{\frac{1}{2b}\xi_i\eta_i\xi\right\}^T \end{bmatrix} \tag{4.3.2}$$

The reduced terms are effectively obtained by replacing the quadratic terms ξ^2 and η^2 in the twisting strain energy:

$$\{x_{xy}\}=$$

$$\left[\left\{-\frac{1}{4ab}\xi_i\eta_i(3\xi^2+3\eta^2-4)\right\}^T \left\{\frac{-1}{4a}\xi_i(3\eta^2+2\eta_i\eta-1)\right\}^T \left\{\frac{1}{4b}\eta_i(3\xi^2+2\xi_i\xi-1)\right\}^T\right]\begin{Bmatrix} w \\ \theta_x \\ \theta_y \end{Bmatrix} \tag{4.3.3}$$

by the constant $\frac{1}{3}$, the value at the four point integration stations.

4.4 *Curvature matrix of the stiffener element*

Double differentiation of the shape functions for the stiffener (3.4.1) gives linearly varying curvatures as below.

$$\chi=\frac{-\partial^2 w}{\partial x^2}=[FS]\begin{Bmatrix} w \\ \theta_y \end{Bmatrix}^e \tag{4.4.1}$$

where

$$\theta_y=\frac{\partial w}{\partial x}$$

and

$$[FS]=\left[\left\{\frac{\bar{3}}{2a^2}\xi_i\xi\right\}^T \left\{-\frac{1}{2a}(3\xi+\xi_i)\right\}^T\right] \tag{4.4.2}$$

4.5 *Slope matrix of the plate element*

This is obtained by differentiating the restricted cubic shape function 3.3.2, which gives slopes as high as cubic. Now

$$\{\theta\}=\begin{Bmatrix} \frac{\partial w}{\partial x} \\ \\ \frac{\partial w}{\partial y} \end{Bmatrix}=[G]\begin{Bmatrix} w \\ \theta_x \\ \theta_y \end{Bmatrix} \tag{4.5.1}$$

In order to make the matrix more consistent with the bilinear variation assumed for the in plane effects, these terms should be reduced (using four Gauss stations), to give linear variation in the x and y directions. The effect is to reduce the cubic terms ξ^3 and η^3 by linear terms $\xi/3$ and $\eta/3$ respectively, and the quadratic terms by the constant $\frac{1}{3}$ as before. The full expression for the strain matrix is as given below, but has been modified (4.5.3.) for application to the computer program.

$$[G]=\begin{bmatrix}\{G_{11}\}\{G_{12}\}\{G_{13}\}\\ \{G_{21}\}\{G_{22}\}\{G_{23}\}\end{bmatrix}, \quad \text{where}$$

$$\{G_{11}\}=\left\{-\frac{1}{8a}\xi_i(1+\eta_i\eta)(3\xi^2+\eta^2-\eta_i\eta-3)\right\}^T$$

$$\{G_{12}\}=\left\{\frac{b}{8a}\xi_i\eta_i(1+\eta_i\eta)(1-\eta^2)\right\}^T$$

$$\{G_{13}\}=\{\tfrac{1}{8}(1+\eta_i\eta)(3\xi^2+2\xi_i\xi-1)\}^T$$

$$\{G_{21}\}=\left\{-\frac{1}{8b}\eta_i(1+\xi_i\xi)(3\eta^2+\xi^2-\xi_i\xi-3)\right\}^T$$

$$\{G_{22}\}=\{-\tfrac{1}{8}(1+\xi_i\xi)(3\eta^2+2\eta_i\eta-1\}^T$$

$$\{G_{23}\}=\left\{\frac{-a}{8b}\xi_i\eta_i(1+\xi_i\xi)(1-\xi^2)\right\}^T \tag{4.5.2}$$

An explicit expression has been derived [21] for the strain matrix using the above mentioned smoothing techniques and is given below:

$$[G]=\begin{bmatrix}\left\{\frac{\xi_i}{12a}(4\eta_i\eta+3)\right\}^T & \left\{\frac{b}{12a}\xi_i\eta_i(1+\eta_i\eta)\right\}^T & \{\tfrac{1}{4}\xi_i\xi(1+\eta_i\eta)\}^T\\ \left\{\frac{\eta_i}{12b}(4\xi_i\xi+3)\right\}^T & \{-\tfrac{1}{4}\eta_i\eta(1+\xi_i\xi)\}^T & \left\{-\frac{a}{12b}\xi_i\eta_i(1+\xi_i\xi)\right\}^T\end{bmatrix} \tag{4.5.3}$$

4.6 *Slope matrix of the stiffener element*

Differentiating equation 3.4.1.

$$\theta_y=\frac{\partial w}{\partial x}=[GS]\begin{Bmatrix}w\\ \theta_y\end{Bmatrix}^e \tag{4.6.1}$$

where

$$[GS] = \left[\left\{ \frac{3\xi_i}{4a}(1-\xi^2) \right\}^T \left\{ \tfrac{1}{4}(3\xi^2 - 1 + 2\xi\xi_i) \right\}^T \right] \tag{4.6.2}$$

Adopting the approach for the plate, this quadratic relationship is replaced by a linear smoothed function through the two-point Gauss stations

$$\left(\xi = \pm \frac{1}{\sqrt{3}} \right)$$

so that

$$[GS] = \left[\left\{ \frac{\xi_i}{2a} \right\}^T \left\{ \frac{\xi\xi_i}{2} \right\}^T \right] \tag{4.6.3}$$

5 Plasticity in the plate element

5.1 *Ilyushin's approximate yield criterion*

In his treatise on plasticity in 1948, Ilyushin [16] expresses the yield criterion in terms of stress resultants for the general case of shells obeying Von Mises criterion of yield, where the basic assumptions discussed in Section 2 have been adopted. The material is assumed to be incompressible and a deformation plasticity law is employed which is still applicable when a flow rule is used [22].

Now, if M_x, M_y, M_{xy} are the bending moments and torsional moment as described in Fig. 8, and N_x, N_y, N_{xy} are equal to the axial stresses and shear stress multiplied by the plate thickness with directions as in Fig. 8, he defines quadratic stress intensities N_e, M_e and MN_e, where

$$\begin{aligned} N_e &= N_x^2 + N_y^2 - N_x N_y + 3N_{xy}^2 \\ M_e &= M_x^2 + M_y^2 - M_x M_y + 3M_{xy}^2 \\ MN_e &= M_x N_x + M_y N_y - \tfrac{1}{2}M_x N_y - \tfrac{1}{2}M_y N_x + 3M_{xy} N_{xy} \end{aligned} \tag{5.1.1}$$

and non dimensionalises them with respect to the uniaxial yield force $N_0 (= \sigma_0 t)$ and uniaxial yield moment $M_0 (= \sigma_0 t^2/4)$. The non-dimensionalised quadratic stress intensities are derived as complex functions of equivalent strain e_{i1} on the top surface, e_{i2} on the bottom surface and the minimum (absolute) value e_{i0}. The yield condition takes the form:

$$F(N_e, M_e, MN_e) = 0 \tag{5.1.2}$$

Ilyushin derived an approximate (simplified) yield surface where the parameters e_i have been eliminated, resulting in

$$f = \frac{N_e}{N_0^2} + \frac{M_e}{M_0^2} + \frac{s}{\sqrt{3}} \frac{MN_e}{M_0 N_0} \leq 1 \tag{5.1.3}$$

where

$$s = \frac{MN_e}{|MN_e|}$$

Various other approximations have been proposed by other authors and reviewed by Robinson [22] who concluded that the above approximation was the best of the linear surfaces. He shows that the error in Ilyushin's approximation is 6% on the safe side and $3\frac{1}{2}\%$ on the unsafe side. Crisfield [15] applied Von Mises yield criterion with five Gaussian integration stations through the plate thickness. On comparing identical solutions on small plate examples with Ilyushin's yield criterion be observed a significant reduction (up to 60%) in the computer time, in addition to the large reduction in computer storage. Although Crisfield has further modified the yield criterion to account for the initial loss of stiffness following first yield of a fibre, the author's present formulation adheres strictly to Ilyushin's approximate yield criterion.

It may be noted that the above criteria apply with reference to the mid-surface of the plate. Therefore, if the mid-surface of the plate is eccentric to the datum (see Fig. 1), the stress resultants have to be referred to the mid-surface for use in equation 5.1.3.

5.2 *Tangential elasto-plastic modular matrices*

In the absence of yielding, the elastic modular matrix for an isotropic plate is given by:

$$[D] = \frac{E}{1-\nu^2}\begin{bmatrix} 1 & \nu & 0 \\ \nu & 1 & 0 \\ 0 & 0 & \dfrac{1-\nu}{2} \end{bmatrix} \tag{5.2.1}$$

As discussed earlier, for the treatment of plasticity all stresses and strains in the plate are transformed to the plate mid-surface. After the treatment, they are converted back to the datum.

The incremental elastic stress strain laws are given by Hooke's Law as

$$\begin{aligned} \{\Delta N^1\} &= t[D]\{\{\Delta\varepsilon_t^1\} - \{\Delta\varepsilon_p^1\}\} \\ \{\Delta M^1\} &= t^3/12[D]\{\{\Delta\chi_t^1\} - \{\Delta\chi_p^1\}\} \end{aligned} \tag{5.2.2}$$

where $\{\Delta N^1\}$ and $\{\Delta M^1\}$ are the incremental generalised stress resultants at the plate mid-surface, defined as:

$$\{\Delta N^1\} = \int_{-t/2}^{t/2} \{\Delta\sigma\}\, dZ \quad \text{and} \quad \{\Delta M^1\} = \int_{-t/2}^{t/2} Z\{\Delta\sigma\}\, dZ$$

Z = distance from the mid-surface

$\{\Delta\varepsilon_t^1\}, \{\Delta\chi_t^1\}$ = total strain and curvature increments respectively, at the plate mid-surface

$\{\Delta\varepsilon_p^1\}$, $\{\Delta\chi_p^1\}$ = plastic strain and curvature increments respectively, at the plate mid-surface and

t = plate thickness

$\{\Delta\varepsilon_t^1\}$ and $\{\Delta\chi_t^1\}$ are obtained from $\{\Delta\varepsilon_t\}$ and $\{\Delta\chi_t\}$ (at the datum) as follows:

$$\begin{aligned}\{\Delta\varepsilon_t^1\} &= \{\Delta\varepsilon_t\} + Z_p\{\Delta x_t\}\\ \{\Delta\chi_t^1\} &\approx \{\Delta\chi_t\}\end{aligned} \tag{5.2.3}$$

where

Z_p = eccentricity of the plate mid-surface from the datum plane.

If plastic flow occurs, the generalised stress resultants remain on the yield surface and $\delta f = 0$. Therefore, from equation 5.1.3

$$\delta f = \left\{\frac{1}{t^2}\left\{\frac{\partial N_e}{\partial N}\right\} + \frac{2s}{\sqrt{3t^3}}\left\{\frac{\partial M_e}{\partial M}\right\}\right\}^T \{\Delta N\} + \left\{\frac{2s}{\sqrt{3t^3}}\left\{\frac{\partial N_e}{\partial N}\right\} + \frac{16}{t^4}\left\{\frac{\partial M_e}{\partial M}\right\}\right\}^T \{\Delta M\} = 0 \tag{5.2.4}$$

In order to avoid discontinuity in the partial derivate of f as $MN_e \to 0$, s is made zero when

$$MN_e < 10^{-4} \times \frac{\sqrt{3t^3\sigma_0^2}}{4}, \text{ (i.e. very small)}$$

Assuming that 5.1.3 is a plastic potential so that the plastic strain rates are proportional to their partial derivates,

$$\begin{aligned}\{\Delta\varepsilon_p^1\} &= \lambda\{f_n\}\\ \{\Delta\chi_p^1\} &= \lambda\{f_m\}\end{aligned} \tag{5.2.5}$$

where

$$\begin{aligned}\{f_n\} &= \frac{1}{t^2}\left\{\frac{\partial N_e}{\partial N}\right\} + \frac{2s}{\sqrt{3t^3}}\left\{\frac{\partial M_e}{\partial M}\right\}\\ \{f_m\} &= \frac{2s}{\sqrt{3t^3}}\left\{\frac{\partial N_e}{\partial N}\right\} + \frac{16}{t^4}\left\{\frac{\partial M_e}{\partial M}\right\}\end{aligned} \tag{5.2.6}$$

λ may be defined as a plastic strain rate multiplier, which when assuming a negative value, signifies unloading from the yield surface. Making use of 5.2.2, 5.2.5 and 5.2.4 we obtain

$$\lambda = \frac{1}{(m+n)}\left(t\{f_n\}^T[D]\{\Delta\varepsilon_t^1\} + \frac{t^3}{12}\{f_m\}^T[D]\{\Delta\chi_t^1\}\right) \tag{5.2.7}$$

where

$$\begin{aligned}n &= t\{f_n\}^T[D]\{f_n\}\\ m &= \frac{t^3}{12}\{f_m\}[D]\{f_m\}\end{aligned} \tag{5.2.8}$$

Therefore, the plastic strain increments maybe related to the total strain increments as

$$\{\Delta\varepsilon_p^1\} = \frac{1}{(\mathrm{m}+\mathrm{n})}\left\{t[G_N][D]\{\Delta\varepsilon_t^1\} + \frac{t^3}{12}[G_{NM}][D]\{\Delta\chi_t^1\}\right| \tag{5.2.9}$$

$$\{\Delta\chi_p^1\} = \frac{1}{(m+n)}\left\{t[G_{NM}]^T[D]\{\Delta\varepsilon_t^1\} + \frac{t^3}{12}[G_M][D]\{\Delta\chi_t^1\}\right\}$$

where

$$\begin{aligned}[G_N] &= \{f_n\}\{f_n\}^T \\ [G_M] &= \{f_m\}\{f_m\}^T \\ [G_{NM}] &= \{f_n\}\{f_m\}^T\end{aligned} \tag{5.2.10}$$

substituting 5.2.9 into 5.2.2 yields the following incremental elasto-plastic stress-strain laws:

$$\begin{aligned}\{\Delta N^1\} &= [C^1]\{\Delta\varepsilon_t^1\} + [cd^1]\{\Delta\chi_t^1\} \\ \{\Delta M^1\} &= [cd^1]^T\{\Delta\varepsilon_t^1\} + [D^1]\{\Delta\chi_t^1\}\end{aligned} \tag{5.2.11}$$

where $[C^1]$, $[D^1]$ and $[cd^1]$ are the tangential elasto-plastic modular matrices about the plate mid-surface, given by:

$$\begin{aligned}[C^1] &= t\left[[D] - \frac{t}{(m+n)}[D][G_N][D]\right] \\ [D^1] &= \frac{t^3}{12}\left[[D] - \frac{t^3}{12(m+n)}[D][G_M][D]\right] \\ [cd^1] &= \frac{-t^4}{12(m+n)}[D][G_{NM}][D]\end{aligned} \tag{5.2.12}$$

now, restating equation 5.2.3

$$\begin{aligned}\{\Delta\varepsilon_t^1\} &= \{\Delta\varepsilon_t\} + Z_p\{\Delta\chi_t\} \\ \{\Delta\chi_t^1\} &= \{\Delta\chi_t\}\end{aligned}$$

where

Z_p = eccentricity of the plate mid-surface from the datum line.

The incremental generalised stress resultants $\{\Delta N\}$ and $\{\Delta M\}$ with respect to the datum line are given by

$$\begin{aligned}\{\Delta N\} &= \int_{Z_p - t/2}^{Z_p + t/2}\{\Delta\sigma\}\,\mathrm{d}Z = \{\Delta N^1\} \\ \{\Delta M\} &= \int_{Z_p - t/2}^{Z_p + t/2} Z\{\Delta\sigma\}\,\mathrm{d}Z = \{\Delta M^1\} + Z_p\{\Delta N^1\}\end{aligned} \tag{5.2.13}$$

substituting 5.2.3 and 5.2.13 into 5.2.11 yields the following incremental elasto-plastic stress strain laws.

$$\begin{aligned}\{\Delta N\} &= [C^*]\{\Delta\varepsilon_t\} + [cd]\{\Delta\chi_t\} \\ \{\Delta M\} &= [cd]^T\{\Delta\varepsilon_t\} + [D^*]\{\Delta\chi_t\}\end{aligned} \tag{5.2.14}$$

where $[C^*]$, $[D^*]$ and $[cd]$ are tangential elasto-plastic modular matrices, given by:

$$\begin{aligned}[C^*] &= [C^1] \\ [D^*] &= [D^1] + 2Z_p[cd^1] + Z_p^2[C^1] \\ [cd] &= [cd^1] + Z_p[C^1]\end{aligned} \tag{5.2.15}$$

These tangential elasto-plastic modular (3×3) matrices are each functions of the current stress resultants (N_x, N_y, N_{xy}, M_x, M_y, M_{xy}) and the plate eccentricity Z_p.

In the absence of plasticity,

$$\begin{aligned}[C^*] &= t[D] \\ [D^*] &= \frac{t^3}{12}[D] + Z_p^2 t[D] \left(= \frac{t^3}{12}[D], \quad \text{if} \quad Z_p = 0\right) \\ [cd] &= Z_p t[D] (= 0, \quad \text{if} \quad Z_p = 0)\end{aligned} \tag{5.2.16}$$

For consistency, these modular matrices are derived at each Gauss point of each element.

6 Plasticity in the stiffener element

In this section, the second moment of area refers to the neutral axis of the stiffener. Also, the simplicity of the treatment does not allow elastic unloading to occur.

6.1 *Unaxial yield criterion*

The stress at any level "Z" from the datum line is given by:

$$\sigma_Z = \frac{N^1}{A} + \frac{M}{I + AZ_s^2} Z \tag{6.1.1}$$

where

Z_s = eccentricity of the stiffener neutral axis from the datum
N^1 = axial load in the stiffener
M = bending moment in the stiffener about the datum
A = cross-sectional area
I = second moment of area of stiffener about the neutral axis

The yield condition is given by:

$$f = \frac{\sigma_Z^2}{\sigma_0^2} \leq 1 \tag{6.1.2}$$

where

σ_0 = yield stress in the stiffener.

Torsional stresses have been ignored in the above assumption.

6.2 *Stress-strain relationship*

In the absence of yielding the elastic stiffnesses are given by EA and EI, where E is the modulus of elasticity of the stiffener.

With the inception of plasticity in the stiffener, the area and second moment of area for the elastic and plastic regions require separate treatment. If A_{el} and I_{el} are properties in the elastic regions and A_{pl} and I_{pl} in the plastic regions, the total stiffnesses are given by:

$$\begin{aligned} EA &= EA_{el} + E^* A_{pl} \\ EI &= EI_{el} + E^* I_{pl} \end{aligned} \tag{6.2.1}$$

where

E^* = the plastic modulus, to include strain hardening or strain softening.

Since a linear elastic-perfectly plastic stress-strain behaviour is assumed, $E^* = 0$.

For convenience in the numerical treatment, total axial strain ε^1 and total curvature χ^1 at the stiffener neutral axis are used. Therefore, the total strain at any level Z (see Fig. 1) is given by:

$$\begin{aligned} \varepsilon_Z &= \varepsilon^1 + (Z - Z_s)\chi^1 \\ \chi_Z &\approx \chi_Z^1 \end{aligned} \tag{6.2.2}$$

The stress at any level Z is given by:

$$\sigma_Z = E\varepsilon_Z$$

where,

$$-\sigma_0 \leq \sigma_Z \leq \sigma_0 \tag{6.2.3}$$

and

σ_0 = yield stress

In the limiting situation, when $\sigma_Z = \pm \sigma_0$, the top and bottom limits of Z within which the stiffener is elastic, are given by:

$$\begin{aligned} Z_t &= \frac{\sigma_0}{E\chi} - \frac{\varepsilon}{\chi} \\ Z_b &= \frac{-\sigma_0}{E\chi} - \frac{\varepsilon}{\chi} \end{aligned} \tag{6.2.4}$$

Therefore, total axial force at the neutral axis

$$N^1 = \Sigma\,(\sigma_Z t_Z b_Z) \tag{6.2.5}$$

total bending moment about the neutral axis

$$M^1 = \Sigma\,(\sigma_Z t_Z b_Z Z) \tag{6.2.5}$$

where t_Z and b_Z are thickness and width of a layer of the stiffener and where

$$|\sigma_Z| \leq |\sigma_0|$$

ε^1 and χ^1 (at the neutral axis) are related to total strain (ε) and total curvature (χ) at the datum line as follows:

$$\begin{aligned} \varepsilon^1 &= \varepsilon + Z_s\,\chi \\ \chi^1 &\approx \chi \end{aligned} \tag{6.2.6}$$

where

Z_s = eccentricity of the stiffener neutral axis from the datum

This eccentricity shifts continuously with the introduction of plasticity, because the properties of the plastic regions are ignored ($E^* = 0$). The stress resultants are given by total force at the datum, $N = \Sigma\,(\sigma_Z t_Z b_Z)$, total bending moment about the datum,

$$M = \Sigma\,\{\sigma_Z t_Z b_Z\ Z\} = M^1 + Z_s N^1 \tag{6.2.7}$$

With $E^* = 0$, the stress strain laws may be expressed as:

$$\begin{aligned} N^1 &= EA_{el}\varepsilon^1 \\ M^1 &= EI_{el}\chi^1 \end{aligned} \tag{6.2.8}$$

substituting 6.2.6 and 6.2.7 into 6.2.8 gives

$$\begin{aligned} N &= EA_{el}\varepsilon + Z_s EA_{el}\chi \\ M &= Z_s EA_{el}\varepsilon + (EI_{el} + Z_s^2 EA_{el})\chi \end{aligned} \tag{6.2.9}$$

7 **Geometric non linearity** (moderately large displacements)

Geometric non linearity is treated by allowing standard linear forms to be used in an iterative way to obtain the solutions. The formulations for the plate, being more general, are given. The stiffener formulation is similar.

When displacements are not infinitesimal, the lateral displacements are responsible for developing membrane strains, and there is a cross coupling of the two actions. The strains are to be defined in terms of displacements at the datum. Therefore, the displacements at any point in the plate depth are:

$$u_Z = u - Z\frac{\partial w}{\partial x}$$

$$v_Z = v - Z\frac{\partial w}{\partial y} \tag{7.1}$$

where

u and v = displacements at the datum
u_Z and v_Z = displacements at distance Z from the datum

The strains may be written as:

$$\{\varepsilon\} = \{\varepsilon_i\} + \{\varepsilon_l\} + Z\{\chi\} \tag{7.2}$$

where

$$\{\varepsilon_i\} = \begin{Bmatrix} \dfrac{\partial u}{\partial x} \\ \dfrac{\partial v}{\partial y} \\ \dfrac{\partial u}{\partial y} + \dfrac{\partial v}{\partial x} \end{Bmatrix} \tag{7.3}$$

$$\{\varepsilon_l\} = \begin{Bmatrix} \dfrac{1}{2}\left(\dfrac{\partial w}{\partial x}\right)^2 \\ \dfrac{1}{2}\left(\dfrac{\partial w}{\partial y}\right)^2 \\ \left(\dfrac{\partial w}{\partial x}\right)\left(\dfrac{\partial w}{\partial y}\right) \end{Bmatrix} \tag{7.4}$$

and

$$\{\chi\} = \begin{Bmatrix} -\dfrac{\partial^2 w}{\partial x^2} \\ -\dfrac{\partial^2 w}{\partial y^2} \\ \dfrac{2\partial^2 w}{\partial x \partial y} \end{Bmatrix} \tag{7.5}$$

The second term is the non-linear term, and u, v and w are the appropriate displacements at the datum. The non-linear strain components (7.4) can be written as:

$$\{\varepsilon_l\} = \tfrac{1}{2}\begin{bmatrix} \dfrac{\partial w}{\partial x} & 0 \\ 0 & \dfrac{\partial w}{\partial y} \\ \dfrac{\partial w}{\partial y} & \dfrac{\partial w}{\partial x} \end{bmatrix} \begin{Bmatrix} \dfrac{\partial w}{\partial x} \\ \dfrac{\partial w}{\partial y} \end{Bmatrix} = \tfrac{1}{2}[A]\{\theta\} \tag{7.6}$$

Taking the variation of 7.6 we have

$$\Delta\{\varepsilon_l\} = \tfrac{1}{2}[\Delta A]\{\theta\} + \tfrac{1}{2}[A]\{\Delta\theta\} + \tfrac{1}{2}[\Delta A]\{\Delta\theta\} = [A]\{\Delta\theta\} + \{\Delta^2\varepsilon_l\} \tag{7.7}$$

where

$$\{\Delta\theta\} = \begin{Bmatrix} \dfrac{\partial \Delta w}{\partial x} \\ \\ \dfrac{\partial \Delta w}{\partial y} \end{Bmatrix} \tag{7.8}$$

The total incremental strain is therefore given by:

$$\{\Delta\varepsilon\} = \{\Delta\varepsilon_i\} + [A]\{\Delta\theta\} + \{\Delta^2\varepsilon_l\} + Z\{\Delta\chi\} \tag{7.9}$$

where $\{\Delta\varepsilon_i\}$, $\{\Delta^2\varepsilon_l\}$ and $\{\Delta\chi\}$ are obtained from $\{\varepsilon_i\}$, $\{\varepsilon_l\}$, and $\{\chi\}$ by replacing u, v and w by the increments Δu, Δv, and Δw.

This can conveniently be written as

$$\{\Delta\varepsilon\} = \{\Delta\varepsilon_l\} + Z\{\Delta\chi\} \tag{7.10}$$

where

$$\{\Delta\varepsilon_l\} = \{\Delta\varepsilon_i\} + [A]\{\Delta\theta\} + \{\Delta^2\varepsilon_l\} \tag{7.11}$$

$\{\Delta\varepsilon_l\}$ refers to the total strain increment at the datum, (i.e. where $Z = 0$) and not at the plate mid-surface.

The total incremental strain and curvature are used to calculate the stresses from the constitutive stress strain relationships in section 5, and stored at the two by two Gauss points for further analysis.

8 Stiffness formulation

8.1 *Stiffness formulation for the plate*

The variational principle of minimum potential energy is used in the formulation, where the potential energy is stationary with regard to all kinematically admissible variations in displacements from the state of equilibrium. The potential energy of the plate (ignoring body forces) is given by

$$\Pi = U - V \tag{8.1.1}$$

where strain energy

$$U = \int_{\text{vol}} \int \int \left(\int_{\varepsilon = \varepsilon_0}^{\varepsilon_1} \sigma \, \mathrm{d}\varepsilon \right) \mathrm{d}\,\text{vol} \tag{8.1.2}$$

and work due to applied loads

$$V = \int_s P(\delta_1 - \delta_0)\, \mathrm{d}s \tag{8.1.3}$$

An increment of the total potential energy is given by:

$$\Delta\Pi = \int_{\text{vol}}\int\int [\{\sigma\}^T\{\Delta\varepsilon\} + \tfrac{1}{2}\{\Delta\sigma\}^T\{\Delta\varepsilon\}]\ \mathrm{d\ vol} - \int_s (P+\Delta P)\Delta\delta\ \mathrm{d}s - \int_s \Delta P(\delta-\delta_0)\ \mathrm{d}s \tag{8.1.4}$$

where the last term may be ignored, since variations with respect to $\Delta\delta$ makes the term zero.

Substituting 7.10 into 8.1.4 gives

$$\begin{aligned}\Delta\Pi = {} & \int_A\int \{N\}^T\{\{\Delta\varepsilon_i\} + A\{\Delta\theta\}\}\ \mathrm{d}A + \int_A\int \{M\}^T\{\Delta\chi\}\ \mathrm{d}A + \tfrac{1}{2}\int_A\int \{\Delta\theta\}^T[N^*]\{\Delta\theta\}\ \mathrm{d}A \\ & + \tfrac{1}{2}\int_A\int \{\Delta N\}^T\{\{\Delta\varepsilon_i\} + \{\Delta\varepsilon_l^2\} + A\{\Delta\theta\}\}\ \mathrm{d}A + \tfrac{1}{2}\int_A\int \{\Delta M\}^T\{\Delta\chi\}\ \mathrm{d}A - \int_s (P+\Delta P)\Delta\delta\ \mathrm{d}s\end{aligned} \tag{8.1.5}$$

where

$$[N^*] = \begin{bmatrix} N_x & N_{xy} \\ N_{xy} & N_y \end{bmatrix}, \quad \{N\} = \int_{-t/2}^{t/2} \{\sigma\}\ \mathrm{d}z \quad \text{and} \quad \{M\} = \int_{-t/2}^{t/2} z\{\sigma\}\ \mathrm{d}z \tag{8.1.6}$$

Introducing the stress-strain (elasto-plastic) relationship into 8.1.5 gives:

$$\begin{aligned}\Delta\Pi = {} & \tfrac{1}{2}\int_A\int [\{\Delta\varepsilon_i\}^T[C^*]\{\Delta\varepsilon_i\} + \{\Delta\theta\}^T[A]^T[C^*][A]\{\Delta\theta\} + \{\Delta\chi\}^T[D^*]\{\Delta\chi\} \\ & + \{\Delta\theta\}^T[A]^T[cd]\{\Delta\chi\} + \{\Delta\chi\}^T[cd][A]\{\Delta\theta\} + \{\Delta\varepsilon_i\}^T[C^*][A]\{\Delta\theta\} \\ & + \{\Delta\theta\}^T[A]^T[C^*]\{\Delta\varepsilon_i\} + \{\Delta\varepsilon_i\}^T[cd]\{\Delta\chi\} + \{\Delta\chi\}^T[cd]\{\Delta\varepsilon_i\}]\ \mathrm{d}A \\ & + \tfrac{1}{2}\int_A\int \{\Delta\theta\}^T[N^*]\{\Delta\theta\}\ \mathrm{d}A - \oint_s [(U+\Delta U)\Delta u + (V+\Delta V)\Delta v]\ \mathrm{d}s - \\ & - \int_A\int (W+\Delta W)\Delta w\ \mathrm{d}A + \int_A\int [\{N\}^T\{\{\Delta\varepsilon_i\} + [A]\{\Delta\theta\}\} + \{M\}^T\{\Delta\chi\}]\ \mathrm{d}A\end{aligned} \tag{8.1.7}$$

where all terms involving products with $\Delta\varepsilon_l$ (higher than third order polynomials) have been ignored.

Now for stable equilibrium, the stationary value of the potential energy is an absolute minimum, i.e. $\delta(\Delta\Pi) = 0$.

On introducing the strains in terms of the displacements, i.e.

$$\begin{aligned}\{\Delta\varepsilon_i\} &= [H]\begin{Bmatrix}\Delta u \\ \Delta u\end{Bmatrix} \\ \{\Delta\chi\} &= [F]\ \ \{\Delta w\} \\ \{\Delta\theta\} &= [G]\ \ \{\Delta w\}\end{aligned} \tag{8.1.8}$$

into 8.1.7

$$\begin{Bmatrix} U \\ V \\ \{W\} \end{Bmatrix} + \begin{Bmatrix} \Delta U \\ \Delta V \\ \{\Delta W\} \end{Bmatrix} - \begin{Bmatrix} \{\int_A\int [H]^T\{N\}\ \mathrm{d}A\} \\ \\ \{\int\int [[G]^T[A]^T\{N\} + [F]^T\{M\}]\ \mathrm{d}A\} \end{Bmatrix} = [K]\{\Delta\delta\} \tag{8.1.9}$$

The first term is the vector of total external forces $\{P_e\}$ prior to applying incremental loads at the nodes, the second term is the vector of nodal values of the incremental applied forces $\{\Delta P_e\}$, and the third term is the internal load vector $\{P_i\}$. All the vectors now refer to the datum $Z=0$ and not the mid-surface of the plate.

$\{\Delta\delta\}$ is the vector of nodal displacements and K the tangent stiffness matrix, given by

$$[K]=\begin{bmatrix}[K_{pl}][K_c]\\ [K_c]^T[K_b]\end{bmatrix} \tag{8.1.10}$$

where

$$\begin{aligned}
[K_{pl}] &= \text{the in-plane stiffness} = \int\int [H]^T[C^*][H]\,\mathrm{d}A\\
[K_b] &= \text{bending stiffness} =\\
&\quad \int_A\int ([F]^T[D^*][F]+[G]^T[A]^T[C^*][A][G]+[G]^T[N^*][G]+\\
&\quad +[F]^T[cd]^T[A][G]+[G]^T[A]^T[cd][F])\,\mathrm{d}A\\
[K_c] &= \text{the coupled stiffness} =\\
&\quad \int_A\int ([H]^T[C^*][A][G]+[H]^T[cd][F])\,\mathrm{d}A
\end{aligned} \tag{8.1.11}$$

In equation 8.1.9 the term $\{P_e\}-\{P_i\}$ gives the out-balance loads between the externally applied forces and the internal stress resultants calculated from the displacements. When this term vanishes after a number of iterations, exact equilibrium has been achieved for the current load increment $\{\Delta P_e\}$.

According to the formulation so far, the plate element has two in-plane degrees of freedom, u, v and three out-of-plane degrees of freedom, w, θ_x, θ_y at each of its nodal points. For convience in assembly of the elements, the in-plane rotation of the element, θ_z, will be introduced. The displacement functions for in-plane effects have been independent of θ_z, since this value is negligible on account of the high stiffness (in-plane) of the elements. However, if zero terms are introduced in the appropriate rows and columns of the stiffness matrix, coplanar elements immediately become singular on transformation to global co-ordinates, should the global co-ordinates differ from the local ones.

This problem could be avoided at the outset by accounting for the real rotational stiffness in the in-plane displacement functions, which result in higher order elements. The problem can also be overcome by adding an arbitrary quantity to the diagonal term of the stiffness matrix corresponding to the singularity [23]. Zienkiewicz et al. [24] suggested a simpler artifice which has been modified in the present approach for rectangular elements.

The nodal rotation θ_z at any node is assumed to be responsible only for developing resisting couples M_z at all the element nodes. The sum of the couples is always zero to ensure equilibrium and made arbitrarily proportional to the youngs modulus "E", plate thickness "t" and element area "A".

This is described by:

$$\begin{Bmatrix} M_{zi} \\ M_{zj} \\ M_{zk} \\ M_{zl} \end{Bmatrix} = \alpha EAt \begin{bmatrix} 1 & -\frac{1}{3} & -\frac{1}{3} & -\frac{1}{3} \\ -\frac{1}{3} & 1 & -\frac{1}{3} & -\frac{1}{3} \\ -\frac{1}{3} & -\frac{1}{3} & 1 & -\frac{1}{3} \\ -\frac{1}{3} & -\frac{1}{3} & -\frac{1}{3} & 1 \end{bmatrix} \begin{Bmatrix} \theta_{zi} \\ \theta_{zj} \\ \theta_{zk} \\ \theta_{zl} \end{Bmatrix} \tag{8.1.12}$$

where α is an undetermined coefficient. This value has been recommended for arch dams as 3×10^{-2} [24], but is considered unsuitable for plated assemblages due to oscillations about the correct value of the flexural component of longitudinal stress at a web-flange function [25]. This is due to the cross coupling between the fictitious rotational stiffness of the web and the bending stiffness of the flange.

The value of α therefore has to be made as small as the computer would allow without making the solution unstable, and the value of α chosen successfully for the Control Data 6600, (and 7600) with 60 bit words and the DEC-VAX 11/780 minicomputer with 32 bit words was 1.0×10^{-11}.

8.2 *Stiffness formulation for the stiffener*

Following the formulation for the plate, an increment of the total potential energy is given by:

$$\Delta\Pi = \int\int t_Z(\sigma_Z \Delta\varepsilon_Z + \tfrac{1}{2}\Delta\sigma_Z \Delta\varepsilon_Z)\mathrm{d}\quad \text{area} \quad - \int [(P+\Delta P)\Delta\delta - \Delta P(\delta - \delta_0)]\,\mathrm{d}x \tag{8.2.1}$$

where the last term may be ignored, since variation with respect to $\Delta\delta$ makes the term zero.

Substituting 7.10 into 8.2.1 gives

$$\Delta\Pi = \int N\left\{\frac{\partial \Delta u}{\partial x} + \frac{\partial w}{\partial x}\cdot\frac{\partial \Delta w}{\partial x}\right\}\mathrm{d}x + \int M\Delta\chi\,\mathrm{d}x + \tfrac{1}{2}\int N\left(\frac{\partial \Delta w}{\partial x}\right)^2\mathrm{d}x$$

$$+\tfrac{1}{2}\int \Delta N\left(\frac{\partial \Delta u}{\partial x} + \tfrac{1}{2}\left(\frac{\partial \Delta w}{\partial x}\right)^2 + \frac{\partial w}{\partial x}\cdot\frac{\partial \Delta w}{\partial x}\right)\mathrm{d}x + \tfrac{1}{2}\int \Delta M\Delta\chi\,\mathrm{d}x - \int (P+\Delta P)\Delta\delta\,\mathrm{d}x \tag{8.2.2}$$

where N and M are the axial force and bending moment in the stiffener at the datum ($Z=0$).

Introducing the stress-strain relationship into 8.2.2 gives

$$\Delta\Pi = \frac{E}{2}\int\left[\left(\frac{\partial \Delta u}{\partial x}\right)^2 A_{el} + \left(\frac{\partial \Delta w}{\partial x}\right)^2\left(\frac{\partial w}{\partial x}\right)^2 A_{el} + (\Delta\chi)^2(I_{el}E_{el} + Z_s^2 A_{el})\right.$$

$$\left. + 2\frac{\partial \Delta w}{\partial x}\frac{\partial w}{\partial x}\Delta\chi Z_s A_{el} + 2\frac{\partial \Delta u}{\partial x}\frac{\partial \Delta w}{\partial x}\frac{\partial w}{\partial x}A_{el} + 2\frac{\partial \Delta u}{\partial x}\Delta\chi Z_s A_{el}\right]\mathrm{d}x$$

$$+\frac{1}{2}\int\left[\left(\frac{\partial \Delta w}{\partial x}\right)^2 N\right]\mathrm{d}x - (U+\Delta U)\Delta u - \int (W+\Delta W)\Delta w\,\mathrm{d}x$$

$$+\int\left[N\left(\frac{\partial \Delta u}{\partial x} + \frac{\partial w}{\partial x}\frac{\partial \Delta w}{\partial x}\right) + M\Delta\chi\right]\mathrm{d}x \tag{8.2.3}$$

where all terms involving products of $\partial \Delta w/\partial x$ have been ignored. For stable equilibrium, the stationary value of the potential energy is an absolute minimum, i.e. $\delta(\Delta \Pi) = 0$.

On introducing the strains in terms of the displacements, i.e.

$$\begin{aligned} \frac{\partial \Delta u}{\partial x} &= [HS]\{\Delta u\}^e \\ \Delta \chi &= [FS] \begin{Bmatrix} \partial w \\ \Delta \theta_y \end{Bmatrix}^e \\ \frac{\partial \Delta w}{\partial x} &= [GS] \begin{Bmatrix} \Delta w \\ \Delta \theta_y \end{Bmatrix}^e \end{aligned} \tag{8.2.4}$$

into 8.2.3,

$$\begin{Bmatrix} U \\ W \end{Bmatrix} + \begin{Bmatrix} \Delta U \\ \Delta W \end{Bmatrix} - \begin{Bmatrix} \int N[HS]\, \mathrm{d}x \\ \int \left[N \frac{\partial w}{\partial x}[GS] + M[FS] \right] \mathrm{d}x \end{Bmatrix} = [K]\Delta\delta \tag{8.2.5}$$

The first term is the vector of total external forces $\{P_e\}$ prior to applying incremental loads at the nodes, the second term is the vector of nodal values of the incremental applied forces $\{\Delta P_e\}$, and the third term is the internal load vector $\{P_i\}$. All the vectors refer to the datum $Z = 0$ and not the stiffener neutral axis.

$[K]$ is the stiffness matrix, given by

$$[K] = \begin{bmatrix} [K_{pl}] & [K_c] \\ [K_c] & [K_b] \end{bmatrix} \tag{8.2.6}$$

where

$$\begin{aligned} [K_{pl}] &= \text{the in-plane stiffness} = \int EA_{el}[HS]^T[HS]\, \mathrm{d}x \\ [K_b] &= \text{the bending stiffness} = \\ &\int \left[(EI_{el} + Z_s^2 EA_{el})[FS]^T[FS] + \left(N + EA_{el} \left(\frac{\partial w}{\partial x} \right)^2 \right) [GS]^T[GS] \right] \mathrm{d}x \\ &+ \int Z_s EA_{el} \frac{\partial w}{\partial x} \left([FS]^T[GS] + [GS]^T[FS] \right) \mathrm{d}x \\ [K_c] &= \text{the coupled stiffness} = \\ &\int \left[EA_{el} \frac{\partial w}{\partial x}[HS]^T[GS] + Z_s EA_{el}[HS]^T[FS] \right] \mathrm{d}x \end{aligned} \tag{8.2.7}$$

The term $\{P_e\} - \{P_i\}$ in equation 8.2.5 gives the out-of-balance loads between the externally applied forces and the internal stress resultants obtained from the displacements. When this term vanishes after a number of iterations, exact equilibrium has been achieved for the current load increment $\{\Delta P_e\}$.

9 Transformation from local to global coordinates

Each element tangent stiffness matrix, evaluated in local coordinates, has to be transformed into the global coordinate system prior to assembly with the other elements of the structure into an overall structural tangent stiffness matrix. The transformation matrix has to be general purpose to cope with any orientation or combination of elements in three dimensions.

From principles of analytical geometry, if the equation of a plane is written as:

$$Ax + By + Cz + D = 0 \tag{9.1}$$

Then the direction cosines of the normal to the plane (z') can be written as:

$$\begin{aligned}
\lambda_{z'x} &= \frac{A_z}{\sqrt{(A_z^2 + B_z^2 + C_z^2)}} \\
\lambda_{z'y} &= \frac{B_z}{\sqrt{(A_z^2 + B_z^2 + C_z^2)}} \\
\lambda_{z'z} &= \frac{C_z}{\sqrt{(A_z^2 + B_z^2 + C_z^2)}}
\end{aligned} \tag{9.2}$$

now the equation of the plane passing through the specified points, 1, 2, 3 (see Fig. 3) of the plate or stiffener element can be written as:

$$\det \begin{vmatrix} x - x_1 & y - y_1 & z - z_1 \\ x_2 - x_1 & y_2 - y_1 & z_2 - z_1 \\ x_3 - x_1 & y_3 - y_1 & z_3 - z_1 \end{vmatrix} = 0 \tag{9.3}$$

from which

$$\begin{aligned}
A_z &= y_{21} z_{31} - y_{31} z_{21} \\
B_z &= -x_{21} z_{31} + x_{31} z_{21} \\
C_z &= x_{21} y_{31} - x_{31} y_{21}
\end{aligned} \tag{9.4}$$

where

$$\begin{aligned}
x_{21} &= x_2 - x_1 \\
y_{21} &= y_2 - y_1 \\
&\text{etc.}
\end{aligned}$$

A_z, B_z and C_z represent the directional vectors of z' axis.

The equation of a plane passing through line $1 - z'$ and point 2 is given by:

$$\det \begin{vmatrix} x - x_1 & y - y_1 & z - z_1 \\ A_z & B_z & C_z \\ x_2 - x_1 & y_2 - y_1 & z_2 - z_1 \end{vmatrix} = 0 \tag{9.5}$$

and the direction cosines given by:

$$\lambda_{y'x} = \frac{A_y}{\sqrt{(A_y^2 + B_y^2 + C_y^2)}}$$

$$\lambda_{y'y} = \frac{B_y}{\sqrt{(A_y^2 + B_y^2 + C_y^2)}} \tag{9.6}$$

$$\lambda_{y'z} = \frac{C_y}{\sqrt{(A_y^2 + B_y^2 + C_y^2)}}$$

where

$$\begin{aligned} A_y &= B_z z_{21} - C_z y_{21} \\ B_y &= C_z x_{21} - A_z z_{21} \\ C_y &= A_z y_{21} - B_z x_{21} \end{aligned} \tag{9.7}$$

In a similar manner, direction cosines of the x' axis are given by:

$$\lambda_{x'x} = \frac{A_x}{\sqrt{(A_x^2 + B_x^2 + C_x^2)}}$$

$$\lambda_{x'y} = \frac{B_x}{\sqrt{(A_x^2 + B_x^2 + C_x^2)}} \tag{9.8}$$

$$\lambda_{x'z} = \frac{C_x}{\sqrt{(A_x^2 + B_x^2 + C_x^2)}}$$

where

$$\begin{aligned} A_x &= B_y C_z - C_y B_z \\ B_x &= C_y A_z - A_y C_z \\ C_x &= A_y B_z - B_y A_z \end{aligned} \tag{9.9}$$

Therefore, the coordinates of the two systems are related by:

$$\begin{Bmatrix} x'_n \\ y'_n \\ z'_n \end{Bmatrix} = [\lambda] \begin{Bmatrix} x_n - x_1 \\ y_n - y_1 \\ z_n - z_1 \end{Bmatrix} \tag{9.10}$$

where subscript n refers to any of the nodes 1, 2, 3 (Fig. 3) and

$$[\lambda] = \begin{bmatrix} \lambda_{x'x} & \lambda_{x'y} & \lambda_{x'z} \\ \lambda_{y'x} & \lambda_{y'y} & \lambda_{y'z} \\ \lambda_{z'x} & \lambda_{z'y} & \lambda_{z'z} \end{bmatrix} \tag{9.11}$$

The element stiffness matrix expressed in global coordinates is given by:

$$[K] = [T]^T [K'][T] \tag{9.12}$$

where

$[K']$ = the element stiffness matrix expressed in local coordinates
$[T]$ = the transformation matrix
$[T]^T$ = the transpose of $[T]$

Each of the above matrices is a 24 by 24 matrix, where

$$[T] = \begin{bmatrix} [\lambda] & & & & & & & \\ & [\lambda] & & & & & & \\ & & [\lambda] & & & & & \\ & & & [\lambda] & & & \text{null} & \\ & & & & [\lambda] & & & \\ \text{null} & & & & & [\lambda] & & \\ & & & & & & [\lambda] & \\ & & & & & & & [\lambda] \end{bmatrix} \tag{9.13}$$

The element nodal displacements are transformed from the global into local coordinates prior to calculating element stress resultants by the following relationship.

$$\{\delta'\} = [T]\{\delta\} \tag{9.14}$$

10 Special Deep Beam Element

In order to model the stress gradients, buckling deformations and the spread of plasticity to an acceptable degree of accuracy, it is necessary to maintain the fineness of the finite element mesh. At the same time, in order to represent the whole structure with finite elements, conventional modelling would lead to either unacceptably high aspect ratios of the elements or to excessively large numbers of elements. This would be particularly so in the case of long box girders or plate girders, where it may be necessary to produce realistic moment/shear ratios.

The author decided to model special beam elements that could represent the box girder as a beam in those regions (away from the region of interest) were linear elastic behaviour may be assumed. Shear deformation, which is significant in box beams, is also accounted for in this formulation.

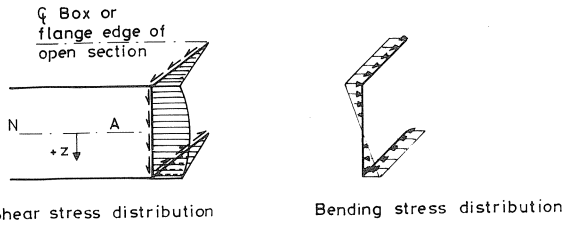

Fig. 4. Stress distribution in special beam elements.

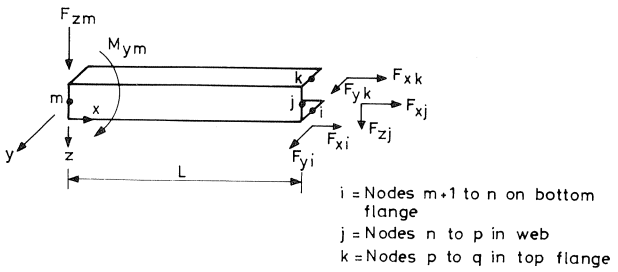

Fig. 5. Basic model of special beam element.

The beam element is modelled to maintain full compatibility of displacements at all nodes on a cross section of the box girder that represents the end of a finite element model and the beginning of a special beam model. Simple Engineering beam theory is used, giving a linear in-plane stress due to bending, and a shear stress distribution as shown in Fig. 4. Fig. 5 shows the special beam element with the arrows representing the positive signs adopted. "i" represents a typical node in the bottom flange, "j" a typical node in the web, and "k" a typical node in the top flange.

Now, the normal stiffness matrix for a beam element (including shear deformation) is given by (see Fig. 6):

$$\begin{Bmatrix} F_{z1} \\ M_{y1} \\ F_{z2} \\ M_{y2} \end{Bmatrix} = \begin{bmatrix} a & & & \\ b & e & \text{sym} & \\ -a & -b & a & \\ b & g & -b & e \end{bmatrix} \begin{Bmatrix} w_1 \\ \theta_{y1} \\ w_2 \\ \theta_{y2} \end{Bmatrix} \tag{10.1}$$

where

$$a = \frac{EI}{(1+2n)} \frac{12}{L^3} \qquad e = \frac{EI}{(1+2n)} \frac{4}{L} \frac{(1+n)}{2}$$

$$b = \frac{EI}{(1+2n)} \frac{6}{L^2} \qquad g = \frac{EI}{(1+2n)} \frac{2}{L} \frac{(1-n)}{4}$$

dimensionless constant

$$n = \frac{6EI}{kAGL^2}$$

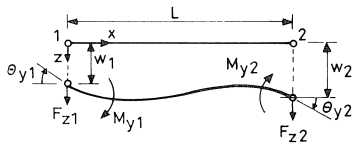

Fig. 6. Beam sign convention for special beam element.

where

kA = total shear area (area of webs)
E = modulus of elasticity
I = second moment of area of beam
G, modulus of rigidity = $E/2(1+v)$
v = Poisson's ratio
L = length of beam element

Equation 10.1 is modified to give the appropriate proportion of shear forces and longitudinal forces at the nodes $\Sigma_i, \Sigma_j, \Sigma_k$ of the finite element cross section as follows, when the end 2 in Fig. 6 is replaced by the finite element nodes as in Fig. 5. Node $m < i, j$ or k i.e. m represents end 1.

If m were a higher node number, a transformation would be required of 10.2 which would change the signs of coefficients containing "b".

$$\begin{Bmatrix} F_{zm} \\ M_{ym} \\ F_{xi} \\ F_{yi} \\ F_{xj} \\ F_{zj} \\ F_{xk} \\ F_{yk} \end{Bmatrix} = \begin{matrix} \\ k_1 \\ -k_2 \\ k_1 \\ k_3 \\ k_1 \\ k_2 \end{matrix} \begin{bmatrix} a & & & & & & & \\ b & e & & & & & & \\ b & g & e & & & & & \\ -a & -b & -b & a & & & & \\ b & g & e & -b & e & & & \\ -a & -b & -b & a & -b & a & & \\ b & g & e & -b & e & -b & e & \\ -a & -b & -b & a & -b & a & -b & a \end{bmatrix} \begin{matrix} \\ k_1 \\ -k_2 \\ k_1 \\ k_3 \\ k_1 \\ k_2 \end{matrix} \begin{Bmatrix} W_m \\ \theta_{ym} \\ u_i \\ v_i \\ u_j \\ w_j \\ u_k \\ v_k \end{Bmatrix} \tag{10.2}$$

where k_1, k_2 and k_3 are the factors to be applied to the matrix in row and column multiplication in order to obtain the nodal stiffness that will be added to the global stiffness matrix. The values of k_1, k_2 and k_3 are dependent on the shear and bending stress distribution of Fig. 4, and vary in sign and magnitude for each node.

The factors have been derived as:

$$k_1 = \frac{-I_n}{\bar{z}I}$$

$$k_2 = \frac{\bar{l}}{I} t_f h\bar{y} \tag{10.3}$$

$$k_3 = \frac{Bht_f\bar{l}}{I} + \left[\{h - t_{f/2}\}^2 - \bar{z}^2\right] \frac{t_w\bar{l}}{I} - \frac{t_w\bar{l}^3}{12I}$$

where

$\bar{z}$ = distance from neutral axis to node in question (+ve downwards in Fig. 5)
$\bar{y}$ = y coordinate from "beam" controid to node in question on flange
$\bar{l}$ = length of wall representing node number in question
t_f = thickness of flange under consideration
t_w = thickness of web under consideration

h = height from neutral axis of beam to flange mid thickness, the flange being on the same side of the neutral axis as the node in question

B = distance from centroid of box or edge of plate girder or channel to web mid thickness in question

I = second moment of area of "beam" about its neutral axis

I_n = second moment of area of section of beam represented by node in question, about the neutral axis of the beam

The above factors ensure the shear and bending stress distribution in Fig. 4 in the stiffness formulations. The matrix so formed is added to the global stiffness matrix in the normal manner.

11 Iterative and Incremental Cycle

The Gaussian elimination method is used for the solution of the simultaneous equations. The out of balance load vector vanishes if the internal and external forces are in exact equilibrium for any particular load increment. The flow chart for the program solution (Fig. 7) indicates the various paths that can be taken, shown as loops. The out of balance forces can be iterated upon using a straight incremental solution (loop 1, where $\{P_e\} = \{P_i\}$), an incremental solution with correction for out of balance forces (loop 2), a modified Newton-Raphson interation (loop 3), or a Newton-Raphson iteration, where the choise is left to the user while incrementing the loads or displacements.

While calculating the internal load vector, although nodal stresses extrapolated from the Gauss points are output for convenience, the vector of stress resultants stored at the Gauss stations are used, as the approach is then more consistent with the derivation of the tangential stiffness matrix.

Convergence is monitored by using the Euclidean norm $\|\Delta\delta\| = [\{\Delta\delta_i\}^T\{\Delta\delta_i\}]^{1/2}$ of the iterative deflections and compared with the Euclidean norm of the cumulative incremental deflection until the last iteration. This ratio is expressed as a percentage, and convergence is deemed to have been satisfied if it is of the order of one percent.

The use of this iterative approach does not always guarantee convergence, and sometimes a combination of two or more methods of solution (incremental, Newton-Raphson etc.) is necessary. It may well be that a judicious combination of the Newton-Raphson and incremental schemes will give optimum economy. Therefore, the scheme adopted by the author allows any one of a combination of the schemes to be chosen while incrementing the loads or deflections. The modified Newton-Raphson procedure adopted allows the stiffness matrix to be updated only at the beginning of each increment, subsequent iterations being carried out using this updated matrix. The whole procedure is thus simplified so that changes from one scheme to another can be easily effected from one increment to another.

It may be borne in mind that the iterations correct for approximations in the linearised treatment of large deflection (geometric non-linearity) and plasticity (material non-linearity). Also, they correct for any residuals in the loads or deflections that could accu-

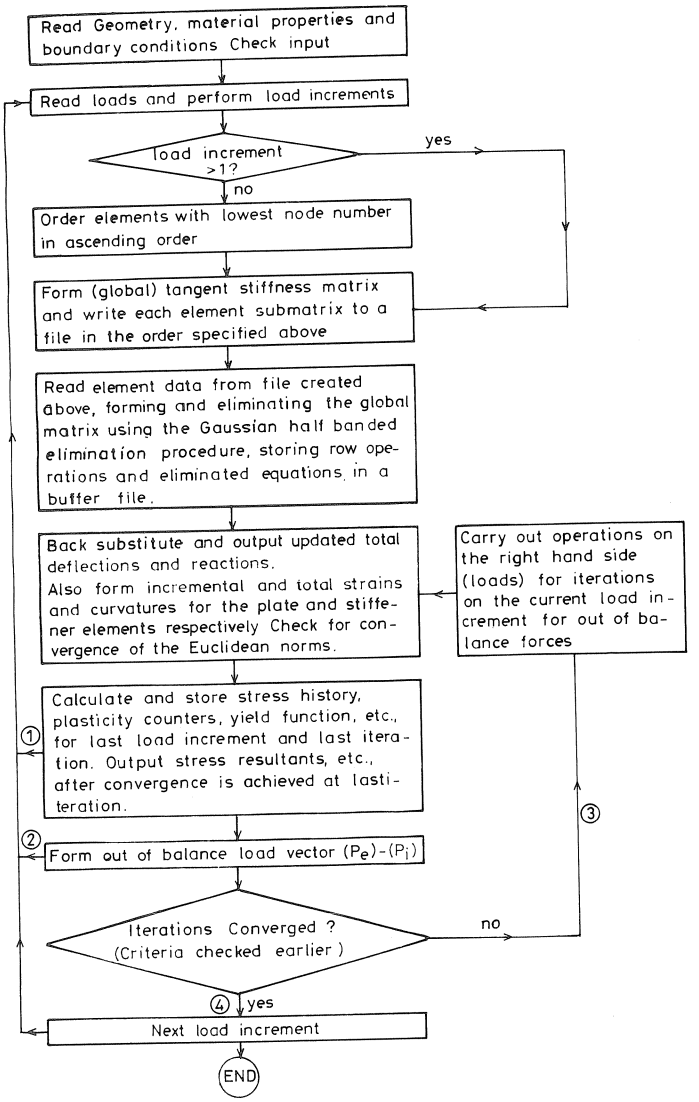

Fig. 7. Flow chart for the computer program "CASPA".

mulate progressively. Therefore, the increments invariably have to be smaller during the plastic stages of loading when the load deflection relationship is highly non-linear, because all the above effects have to be accounted for simultaneously.

12 Monitoring of stress resultants

12.1 *Plate elements*

The stress resultants and the stress history are stored at the two by two Gauss points (w at the datum). Monitoring of the stresses are carried out after transformation to the plate mid-surface. However, the term:

$$\int_A \int [G]^T [A]^T [C^*][A][G] \, dA$$

in equation 8.1.11 (for the plate) strictly requires a three by three integration, since it contains the most highly non-linear terms in x and y in the tangent stiffness matrix. Also, in the elastic stages, no other terms require more than the two by two integration, since the cross coupling elasto-plastic modular matrix $[cd]$ does not exist. In the plastic stages, however, the existence of this modular matrix term brings in further terms which require a three by three Gaussian integration.

Therefore, as a comprise, a two by two Gaussian integration of the complete stiffness matrix is employed for the plate during the elastic increments, and a three by three Gaussian integration during the plastic stages of loading. The values of the terms $[N^*]$, $[C^*]$, $[D^*]$ and $[cd]$ in equation 8.1.11 (for the plate) are then obtained by bilinear extrapolation from the values at the two by two Gauss stations that are already stored or calculated.

The incremental stress resultants are calculated from the constitutive stress strain relationship in equation 5.2.14 and added to the total sum of all incremental stress resultants. The modular matrices are resolved from the average value of the stress resultants at the last increment and the last iteration i.e.

$$\begin{aligned} M_{av} &= \tfrac{1}{2}(M_{i-1} + M_{i,t-1}) \\ N_{av} &= \tfrac{1}{2}(N_{i-1} + N_{i,t-1}) \end{aligned} \tag{12.1.1}$$

where

M_{i-1}, N_{i-1} are stress resultants at the previous load or deflection increments

$M_{i,t-1}$, $N_{i,t-1}$ are stress resultants from the last iteration of the present increment

The total stress resultants (sum of all increments) are given by:

$$\begin{aligned} N_{i,t} &= N_{i-1} + [C^*]\{\Delta\varepsilon_t\} + [cd]\{\Delta\chi_t\} \\ M_{i,t} &= M_{i-1} + [cd]\{\Delta\varepsilon_t\} + [D^*]\{\Delta\chi_t\} \end{aligned} \tag{12.1.2}$$

where

$[C^*]$, $[cd]$ and $[D^*]$ are functions of M_{av} and N_{av}

Points that are elastic at the start of an increment, but become plastic during iterations are dealt with as in reference [17]. If

f_{i-1} = elastic value of yield function at the end of the i-th increment,
f_i = plastic value at the current iteration of the current increment,

the strain increments that would cause the stress resultants to remain elastic could be approximated by

$$A = (1 - f_{i-1})/(f_i - f_{i-1}) \tag{12.1.3}$$

The stress resultants required to reach the yield surface are given by:

$$\begin{aligned}\{\bar{N}\} &= \{N_{i-1}\} + A[\{N_{i,1}\} - \{N_{i-1}\}] \\ \{\bar{M}\} &= \{M_{i-1}\} + A[\{M_{i,1}\} - \{M_{i-1}\}]\end{aligned} \tag{12.1.4}$$

where $\{N_{i,1}\}$ and $\{M_{i,1}\}$ are the first estimate of the "elastic" stress resultants given by:

$$\begin{aligned}\{N_{i,1}\} &= \{N_{i-1}\} + [D]\{\Delta\varepsilon_t\} \\ \{M_{i,1}\} &= \{M_{i-1}\} + [D]\{\Delta\chi_t\}\end{aligned} \tag{12.1.5}$$

A better estimate of the stress resultants is given by:

$$\begin{aligned}\{N_{i,2}\} &= \{\bar{N}\} + (1-A)[[C^*]\{\Delta\varepsilon_t\} + [cd]\{\Delta\chi_t\}] \\ \{M_{i,2}\} &= \{\bar{M}\} + (1-A)[[cd]\{\Delta\varepsilon_t\} + [D^*]\{\Delta\chi_t\}]\end{aligned} \tag{12.1.6}$$

where

$[C^*]$, $[cd]$ and $[D^*]$ are functions of $\{\bar{N}\}$ and $\{\bar{M}\}$

Subsequent iterations finally stabilise the values of the stress resultants and modular matrices at a fully converged value.

Due to the finite nature of the load or deflection increments adopted, violation of the yield surface occurs, and the tangency condition δf, (equation 5.2.4) is no longer zero. The stress resultants are therefore adjusted by a factor C, where:

$$C = \frac{1.0}{f_i} \tag{12.1.7}$$

where

f_i=value of the yield function (greater than 1.0) so that the stress resultants are again on the yield surface

Should any unloading of the stress resultants from the yield surface occur, the plastic strain rate multiplier λ (equation 5.2.5 and 5.2.7) becomes negative. In such an event, the stress resultants during the iteration are moved away from the yield surface by making $f < 1.0$ (say 0.995), i.e. reducing the stress resultants by a factor c where:

$$c = \frac{0.995}{f_i} \tag{12.1.8}$$

and assuming the Gauss point to be elastic in the next iteration.

A pointer is kept of the Gauss points which are plastic (full section depth) as defined by Ilyushin's approximate theory, where $f = 1.0$. Also the positions where fibre yield has occurred are stored for each increment from the relationship (see equation 5.1.1 for definitions)

$$f_y = \frac{N_e}{t^2\sigma_0^2} + \frac{12sMN_e}{t^3\sigma_0^2} + \frac{36M_e}{t^4\sigma_0^2} \tag{12.1.9}$$

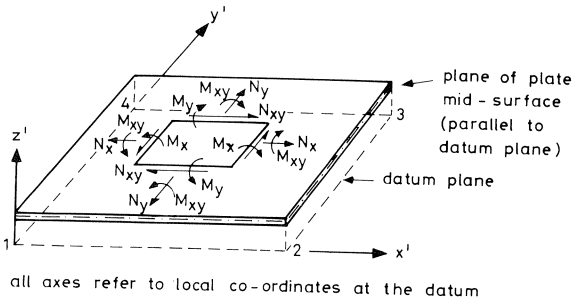

Fig. 8. Stress resultants of plate element with reference to the datum.

where fibre yield has occurred if the yield function f is:

$$f_y \leq f < 1.0 \tag{12.1.10}$$

The stress resultants at the nodes of each element are output by a bilinear extrapolation from the two by two Gauss stations. Therefore, smoothing of the numerically discontinuous model is not carried out by averaging nodal stress resultants. Should such a smoothing solution be required, manual averaging is resorted to.

Such an average does result in serious errors in regions of large stress gradients or where element sizes vary, and therefore interpretation of the stress resultants are left to the user's discretion.

The signs and directions of the stress resultants are given in Fig. 8 where arrows indicate the positive signs.

12.2 *Stiffener elements*

The treatment here is much simpler, because stresses are directly evaluated from total strains, using a simple yield criterion. Therefore, spread of plasticity through the stiffener depth is easily monitored. A pointer is kept of the distance from the datum line to the position (in the depth of the stiffener) where yield has occurred. Stresses are stored at the two Gauss stations with respect to the datum. The stress resultants at the nodes are output by linear extrapolation from the two Gauss stations, as for the plate element. The signs and directions of the stress resultants are as given in Fig. 9, where the arrows indicate the positive signs.

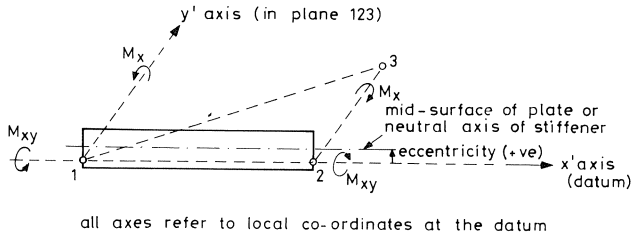

Fig. 9. Stress resultants of stiffener element with reference to the datum.

13 Comparison of established numerical and analytical treatments with the results of computer program CASPA

13.1 *Imperfect plate subjected to uniaxial compression*

Moxham [26, 27] carried out both experimental and theoretical work to obtain an elasto-plastic solution for the above plates.

His work has therefore been used to test the accuracy of the program in the elasto-plastic range.

Moxham [27] used a Ritz approach with eight Fourier coefficients representing the deflected shape of the plate, while the plate had five divisions in its depth. An iterative minimisation method was utilised in finding the stationary energy configuration. Moxham [27] concluded that long plates would deform the approximately square buckles with aspect ratio approximately 0.875. He therefore analysed plates with these aspect ratios, simply supported on the sides in order to predict the behaviour of longer plates.

Although several breadth to thickeness (b/t) ratios were investigated by Moxham, the range chosen for comparison using mild steel plates was a b/t ratio of 55 only. This was because the elastic critical buckling load was close to the squash yield load of the plate, exploiting the full large deflection elasto-plastic capabilities of the program.

Bradfield [28] carried out further theoretical work using Moxham's computer programs, and presented results for varying imperfections for the same plates. The imperfections chosen were sinusoidal along the length and breadth of the plate, the imperfection δ_0 representing the maximum initial deformation in the centre of the plate. In the present work, an initial imperfection of $\delta_0 = 0.005b$ was used, where $b =$ width of the plate. The load shortening curve obtained was satisfactorily sandwiched between the imperfections of $\delta_0 = 0{,}003b$ and $0.01b$ used by Bradfield (see Fig. 10). An imperfection sensitivity plot of Bradfield's results gives an estimated maximum average stress value for δ_0/b of 0,005 equal to $0{,}725\sigma_0$ which compares favourably with the value given for the present work ($0{,}74\sigma_0$). σ_0 represents the yield stress.

13.2 *Square clapmed plate under uniformly distributed load*

Hooke and Rawlings [29] suggest that a permanent set or a limit on the maximum deflection would be a more relevant design criterion in fully clamped plates. This is due to the significantly large reserves of strength possessed by such plates after the onset of yielding. Due to the absence of reliable permanent set data, design procedures have assumed limiting stress conditions instead. They therefore conducted experiments on a clamped plate, the results of which are compared with the large deflection elasto-plastic solution using the program. The poor comparison obtained is due to the inexact boundary conditions simulated by Hook and Rawlings, giving a more flexible plate than the finite element solution. The clamped edges had "pulled in" at various stages (note the reversals in the load deflection plot (Fig. 11) having a significant effect on the plate behaviour.

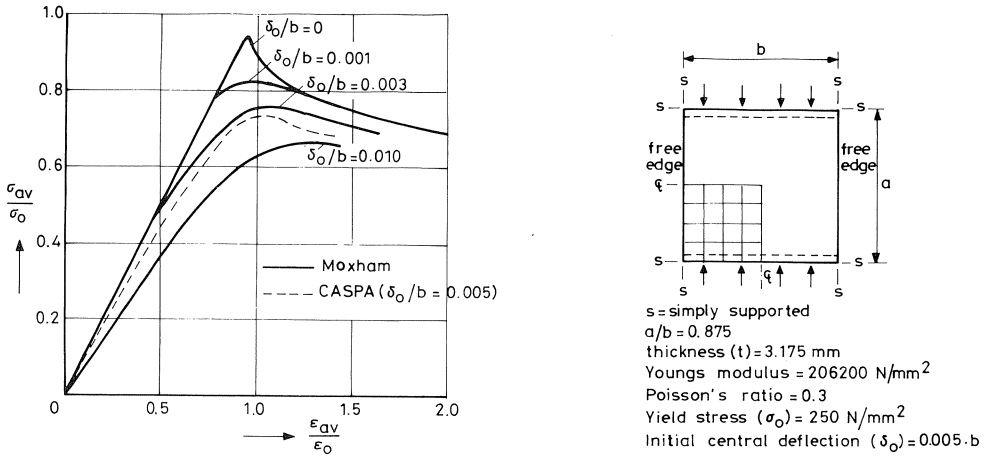

Fig. 10. Relationship between average load and end shortening for a simply supported plate with $b/t = 55$, under uniaxial compression.

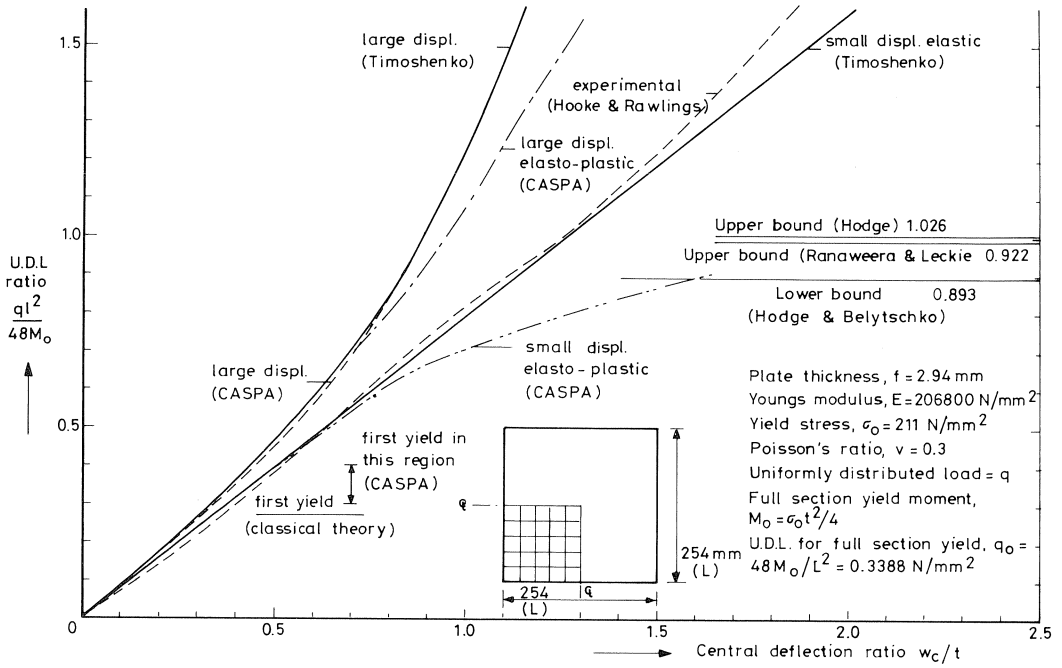

Fig. 11. Relationship between load and lateral central deflection for a square fully clamped plate under uniformly distributed load.

The small deflection elastic and the large deflection elastic finite element results are almost identical with Timoshenko's classical solution. The small deflection elasto-plastic solution lies between the largest lower bound and smallest upper bound solutions provided by Hodge and Belytschko [30] and Ranaweera and Leckie [31]. The author's solution has not been provided over a satisfactory length of the plateau because of the extremely slow convergence in this region. Also, small deflection elasto-plastic solutions are not relevant for the intended use of the program.

13.3 *Imperfect simply supported strut subjected to uniaxial compression*

The accuracy of the program for the elasto-plastic relationship of the stiffener has been calibrated by comparison with work done by Crisfield [32], where he used a Ritz procedure for the analysis, with five Gaussian integration stations through the depth of the strut. The initially deflected shape is represented by a sine wave, as shown in Fig. 12. The relationship between load and out-of-plane deflection using program CASPA compares very favourably with the Ritz method as seen in Fig. 12.

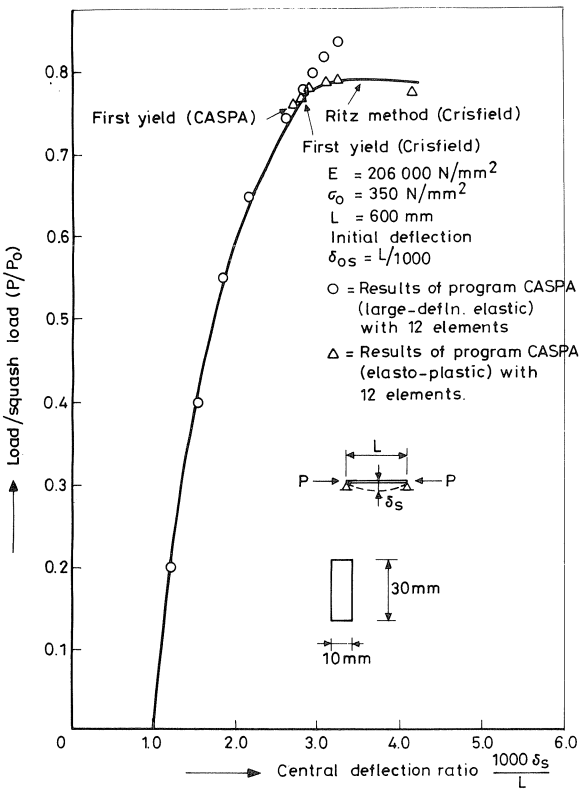

Fig. 12. Relationship between load and out-of-plane deflection for uniaxially compressed simply supported rectangular strut.

14 Comparison of experimental results with results of computerprogram CASPA

14.1 *Experiments at Imperial College, London*

Not many experiments have been conducted on large deflection elasto-plastic behaviour of steel plated assemblages up to collapse, where stresses and deformations have been accurately recorded. This is mainly on account of the expensive fabrication and testing procedures, requiring large testing equipment. In 1972, the first of such large scale tests were carried out at Imperial College, London [33] using four symmetrically loaded unstiffened box girder diaphragms situated at the ends of model box girders. These diaphragms were labelled diaphragms D1, D2 and D3. These have all been investigated in depth by Crisfield and Puthli [4] using two dimensional idealisation, where it was stated hat diaphragm D1 collapsed with pure squash failure. Diaphragm D2 is in the middle range of breadth to thickness ratios (b/t), producing a combination of instability and plastic deformation, and was therefore chosen for the analysis in three dimensions (3D) using the present program.

The experimental diaphragm D2 was located at the end of a model box girder, which has been idealised for analytical purposes as shown in Fig. 13. At some distance away from the Diaphragm D2, a substantially rigid intermediate load bearing diaphragm was provided, over which was positioned a high capacity reaction spherical bearing during testing.

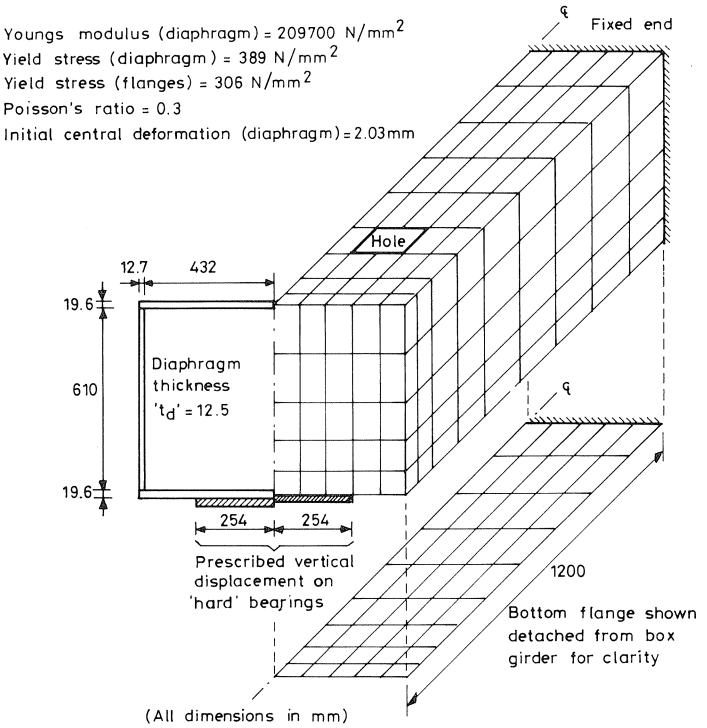

Fig. 13. Structural idealisation, dimensions and mesh for the analysis of the Imperial College experimental box with end diaphragm D2.

This position along the box was represented by the idealised fixed end. Jacks were positioned under a similarly stiff diaphragm further away to provide the balancing moment from the reactions.

Uniformly prescribed displacements were applied to the end diaphragm D2 in the computer analysis at the nodes signifying the bearing. The portion of the box between the end diaphragm D2 and the intermediate diaphragm was given all the measured dimensions and properties of the test specimen, including the square hole positioned on the top flange for access into the box girder.

The computed failure load (2960 kN) was wihin 7% of the experimental value (2770 kN). The discrepancy was partly due to the fact that the Ilyushin's yield criterion adopted gives an upper bound to the collapse load on account of assuming "full-section" yielding in the plate depth. Another reason is that as Dean [33] noted, the ductility in the bearings, lower flange and intervening weld zone caused the peak experimental reaction to move away from the bearing edge towards the centre of the diaphragm. This phenomenon therefore weakens the structure, causing an earlier collapse than anticipated. Curves 1 for the experimental and analytical vertical membrane stress in Fig. 14 indicate the shift in the experimental peak reaction towards the centre of the box during the earlier loading stages. Since the mesh division is too coarse near the edge of the bearing, this behaviour is not observed at higher loads when the stress gradients are very steep (curves 2, Fig. 14).

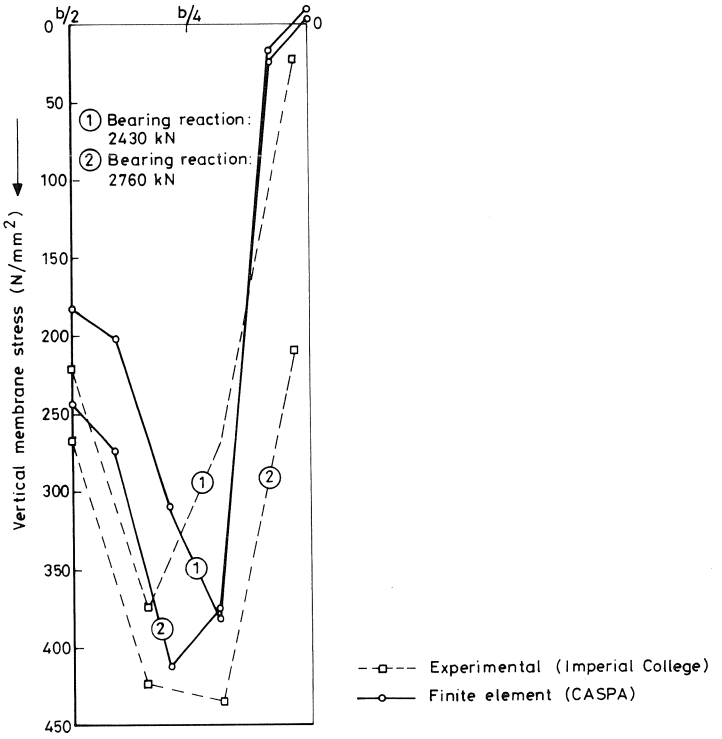

Fig. 14. Vertical membrane stress in diaphragm, 51 mm from the bottom flange.

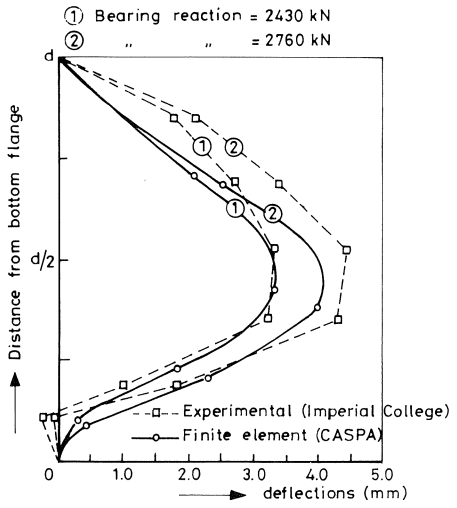

Fig. 15. Deflections under load at the diaphragm centre line.

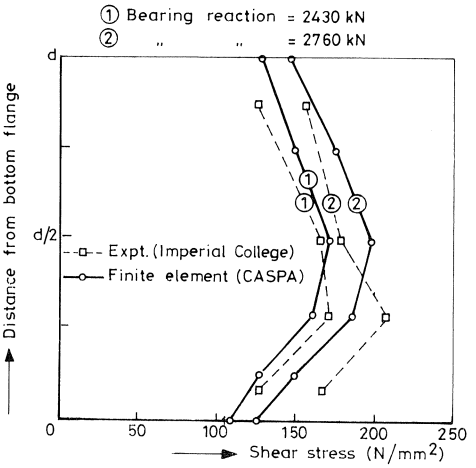

Fig. 16. Web membrane shear stress at 51 mm from the mid-thickness of the diaphragm.

In spite of the scatter in the measured imperfections of the diaphragm D2, the experimental and predicted out of plane deformations up to collapse agree, as shown in Fig. 15.

The idealised out of plane initial imperfection was assumed to be sinusoidal, with an amplitude of 2.03 mm. This was assumed to give the best fit to the measured imperfections. The largest variations in the idealised and measured imperfections were just above the diaphragm bearing and in the top half of the diaphragm. This variation is reflected in the out of plane deformations up to collapse (see Fig. 15). The web shear stress adjacent to the diaphragm D2 for the predicted and experimental cases are also shown, in Fig. 16.

In conclusion, it would appear that the finite element program developed herein has produced results which compare very favourably with these experimental test results.

14.2 *Experiments at Manchester University*

Horne and Narayanan [34, 35] carried out an extended series of tests on the ultimate load capacity of unidirectionally compressed, eccentrically stiffened plates in 1974. In these tests, the initial deformations were forced into square sinusoidal patterns by "dishing" the panels to give nearly identical amplitudes. Residual stresses were also measured and average values (σ_r) presented for the plate and stiffener. Fig. 17 gives the details of the case (specimen D 21) chosen for comparison, where the panels were made from British Structural Grade 43 steel.

The finite element mesh used for the analysis is shown in Fig. 17. The residual stresses were simulated approximately for the analytical treatment by reducing the yield

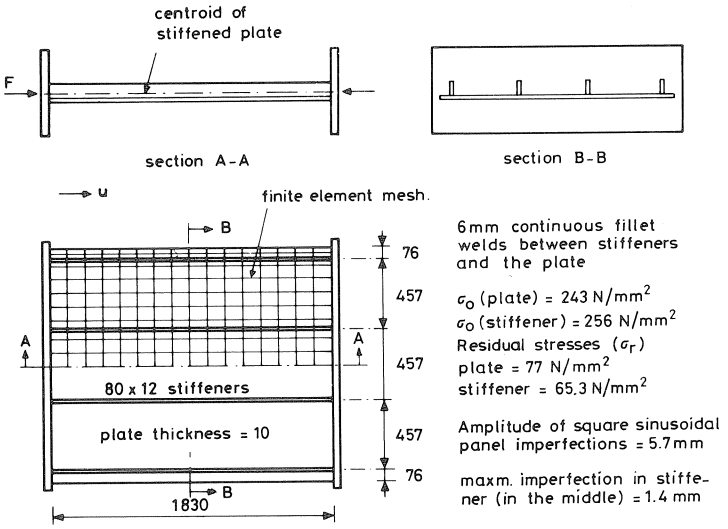

Fig. 17. Pin ended stiffened plate 1524 wide.

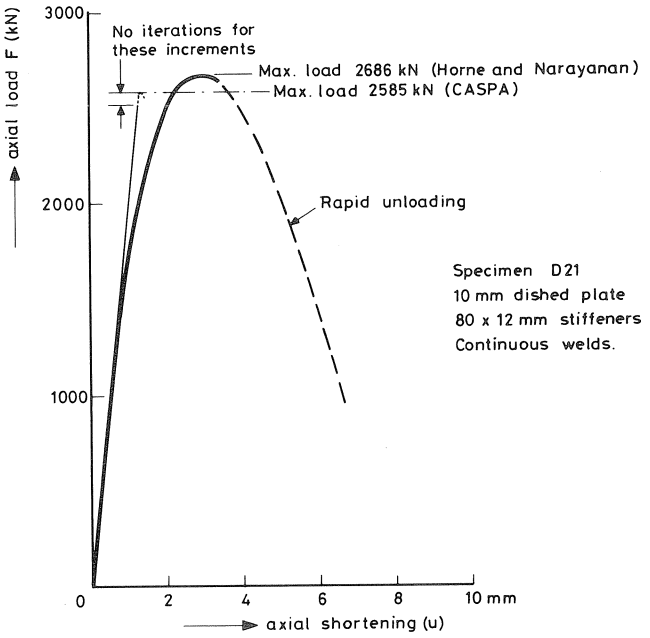

Fig. 18. Load vs axial shortening.

stress in areas with compressive residual stresses (i.e. new yield stress $= \sigma_0 - \sigma_r$) and increasing the yield stress to twice its value in areas of tensile yield. This representation is not accurate and the collapse load obtained (2585 kN) is therefore lower than that observed experimentally (2686 kN). Also, the loss in stiffness due to initial residual compressive stresses is not included with such a treatment, so that non-linearity is not so pronounced in the later stages of loading when its effect is more significant.

Above the total load of 2528 kN, convergence was difficult to achieve because of the proximity to sudden collapse and rapid unloading. The last three increments before collapse were therefore carried out without iterations. Collapse is assumed to occur at the last increment where all diagonal coefficients in the tangent stiffness matrix are positive. Although factors such as approximations in the input data and theory would give variations in the behaviour of the theoretical model, the main reason for deviation from the experimental behaviour is thought to be the approximate representation of residual stresses. It is therefore intended to reanalyse the example after modifying the computer program to include residual stresses correctly.

Bearing in mind that residual stresses have been treated approximately, this analysis has been presented to show that computer program CASPA can also idealise eccentrically stiffened plates and model their behaviour upto and including collapse.

15 Conclusions

A general purpose computer program CASPA has been written for the collapse analysis of stiffened steel plated assemblages. The theory uses a number of economic simplifying approximations. Because some of these approximations allow large savings in computer time and storage, it has been possible to analyse complex stiffened plate structures up to collapse. The computer program has been checked against theoretical and experimental results and good agreement has been found.

The program may be used to investigate the effects of various boundary conditions and initial imperfections on the collapse behaviour of stiffened plate assemblages. Such parametric studies would provide data for the development of simple design rules and insight into the interactive behaviour of stiffened panels that are not necessarily in the same plane.

Although the computer program can be used in its present form, further improvements are desirable. Notably, amendments to incorporate elastic unloading of the stiffeners; modifications in the iterative procedure to allow better convergence in the highly non-linear regions where the tangent stiffness of a structure changes sign; input of residual stresses as initial stresses in the plate and stiffener elements.

16 References

1. Frieze, P. A., P. J. Dowling and R. E. Hobbs, Ultimate load behaviour of plates in compression. An International Conference on Steel Plated Structures, London, Crosby Lockwood Staples, 1977, p. 24.
2. Dowling, P. J., Some approaches to the non-linear analysis of plated structures. Symposium on Non-Linear Techniques and Behaviour in Structural Analysis, Crowthorne, Transport and Road Research Laboratory, SR164 U C 1974, p. 86.
3. Harding, J. E., R. E. Hobbs and B. G. Neal, Ultimate load behaviour of plates under combined direct and shear in-plane loading. An International Conference on Steel Plated Structures, London, Crosby Lockwood Staples, 1977, p. 369.
4. Crisfield, M. A. and R. S. Puthli, A finite element method applied to the collapse analysis of stiffened box girder diaphragms. An International Conference on Steel Plated Structures, London, Crosby Lockwood Staples, 1977, p. 311.
5. Puthli, R. S. and M. A. Crisfield, The strength of stiffened box girder diaphragms. Transport and Road Research Laboratory Supplementary Report no. 353, Crowthorne, U.K., 1977.
6. Evans, M. R., D. M. Porter and K. C. Rockey, Ultimate load behaviour of plate and box girder webs. An International Conference on Steel Plated Structures, London, Crosby Lockwood Staples, 1977, p. 338.
7. Horne, M. R. and R. Narayanan, The design of axially loaded stiffened plates. A.S.C.E. Structural Division 1977.
8. Dwight, J. B. and G. H. Little, Stiffened steel compression flanges - a simpler approach. The Structural Engineer, Vol. 54, December 1976, p. 501.
9. Graves-Smith, T. R., The post buckled behaviour of a thin walled box beam in pure bending. International Journal of Mechanical Sciences, Vol. 14, No. 1, November 1972, p. 711.
10. Frieze, P. A. and P. J. Dowling, Interactive buckling analysis for box sections using dynamic relaxation. International Symposium on Innovative Numerical Analysis in Applied Engineering Science, Versailles, France, 23-27th May 1977.
11. Frieze, P. A., Detailed behaviour of thin walled rectangular hollow beams. International Conference on Thin-Walled Structures, Glasgow University, April 1979.
12. Puthli, R. S., M. A. Crisfield and W. J. Supple, Interactive collapse of plate assemblages in relation to the strength of box girders. Preliminary Report on Stability of Steel Structures, Liège, April 1979, p. 427.
13. Puthli, R. S. The effect of web thickness on the collapse of unstiffened steel box girders. Final report on Stability of Steel Structures, Liège, April 1977, p. 165.
14. Puthli, R. S., W. J. Supple and M. A. Crisfield, Collapse behaviour of rectangular steel box girders. The Structural Engineer, Part B, December 1978, Vol. 56 B, No. 4, p. 75.
15. Crisfield, M. A., Large deflection elasto-plastic buckling analysis of plates using finite elements. Transport and Road Research Laboratory, Report, LR 593, Crowthorne, U.K., 1973.
16. Ilyushin, A. A., Plasticité, Editions Eyrolles, Paris 1965.
17. Zienkiewicz, O. C., The Finite Element Method in Engineering Science. McGraw-Hill, London 1971.
18. Zienkiewicz, O. C. and Y. K. Cheung, The finite element method for analysis of elastic isotropic and orthotropic slabs. Proceedings of the Institution of Civil Engineers, Vol. 28, Paper no. 6726, August 1968, pp. 471-488.
19. Melosh, R. J., Basis for derivation of matrices for the direct stiffness method. Journal of the A.I.A.A., Vol. 1, No. 7, 1963, pp. 1631-1637.
20. Wilson, E. L., R. L. Taylor, W. P. Doherty and J. Ghaboussi, Incompatible displacement models. Proceedings of the O.N.R. Conference on Numerical Methods, Urbana, Illinois, Sept. 1971.
21. Crisfield, M. A., Some approximations in the non-linear analysis of rectangular plates using finite elements. T.R.R.L. Supplementary Report 51UC, 1974.
22. Robinson, M., A comparison of yield surfaces for thin shells. International Journal of Mechanical Sciences, Vol. 13, No. 4, April 1971, pp. 345-354.

23. EISEMAN, K., L. WOO and S. NAMYET, Space frame analysis by matrices and computer. Journal of the Struct. Div. Proc. A.S.C.E., Vol. 88, No. ST6, Paper 3365, Dec. 1962, pp. 245–277.
24. ZIENKIEWICZ, O. C., C. J. PAREKH and I. P. KING, Arch dam analysis by a linear finite element shell solution program. Proceedings of the Symposium on Arch Dams. Institution of Civil Engineers, London 1968.
25. LIM, P. T. K., J. T. KILFORD and K. R. MOFFATT, Finite element analysis of curved box girder bridges. Proceedings of the International Conference on Developments in Bridge Design and Construction, Cardiff 1971 (ed. K. C. Rockey et al.), Crosby Lockwood, London, pp. 264–286.
26. MOXHAM, K. E., Buckling tests on individual welded steel plates in compression. Cambridge University, Technical Report CUE/C-Struct/TR3, 1971.
27. MOXHAM, K. E., Theoretical prediction of the strength of welded steel plates in compression. Cambridge University, Technical Report CUED/C-Struct/TR2, 1971.
28. BRADFIELD, C. D., Further calculations using Moxham's Program. Cambridge University, Department of Engineering, June 1974.
29. HOOKE, R. and B. RAWLINGS, An experimental investigation into the behaviour of clampled, rectangular mild steel plates subject to uniform transverse pressure. Proceedings of the Institution of Civil Engineers, Vol. 42, Jan. 1969, pp. 75–103.
30. HODGE, P. G. and T. BELYTSCHKO, Numerical methods for the limit analysis of plates. Journal of Applied Mechanics, Vol. 35, No. 1, Trans. A.S.M.E., Vol. 90, Series E. Dec. 1968, pp. 796–802.
31. RANAWEERA, M. P. and F. A. LECKIE, Bound methods in limit analysis. Chapter 9 in Conference on Finite Element Techniques in Structural Mechanics, (ed. H. Tottenham and C. Brebbia), University of Southampton, 1970, pp. 259–282.
32. CRISFIELD, M. A., Large-deflection elasto-plastic buckling analysis of eccentrically stiffened plates using finite elements. Transport and Road Research Laboratory Report 725, Crowthorne, U.K., 1976.
33. DEAN, J. A., The collapse behaviour of steel plating subject to complex loading, Ph.D. Thesis, University of London, 1975.
34. HORNE, M. R. and R. NARAYANAN, Ultimate load capacity of longitudinally stiffened panels – A report on panels with $b/t = 48$ and $l/r = 20$ and 40. Simon Engineering Laboratories, University of Manchester, January 1974.
35. HORNE, M. R. and R. NARAYANAN, Further tests on the ultimate load capacity of longitudinally stiffened panels – A report on panels with $b/t = 48$ and 70 and $l/r = 20$, 40 and 90. Simon Engineering Laboratories, University of Manchester, July 1974.